Pergamon

Geochimica et Cosmochimica Acta, Vol. 60, No. 12, pp. 2087–2109, 1996

0016-7037/96 $15.00 + .00

PII S0016-7037(96)00077-4

A convective model of water flow in Mururoa basalts

P. HENRY,[1,*] C. GUY,[1] R. CATTIN,[1] P. DUDOIGNON,[2] J. F. SORNEIN,[1] and Y. CARISTAN[1]

[1]CEA, Laboratoire de Détection et de Geophysique, B.P. 12, 91680 Bruyères le Châtel, France
[2]E.S.I.P., 40 Av. du Recteur Pineau, 86022 Poitiers Cedex, France

(*Received September* 30, 1994; *accepted in revised form February* 26, 1996)

Abstract—Even long after the end of volcanic activity, the background geothermal flux of Mururoa atoll (French Polynesia) maintains fluid convection. We present evidences that interstitial water is continuously renewed in the carbonate platform, as well as in the volcanic basement. In the carbonate rocks, the presence of a karst system allows convective fluxes high enough for the thermal equilibration of the formation with the ocean around. On the contrary, convection in the volcanic basement is, in most places, too slow to cause a measurable disturbance of temperature profiles. Thermal convection models indicate that the average permeability of the volcanic basement cannot be more than a few 10 mD (10^{-14} m^2), implying a residence time of more than 10,000 years. The concentration of Sr in porewaters is used as an indicator of the rock/water ratio and of the residence time of the fluid. Considering the measured permeabilities and the estimated rates of reaction, residence times of more than 1 My, corresponding to average permeabilities of less than 10^{-16} m^2, are unlikely in the studied upper kilometer of the volcano. However, the extrapolation of the rates of dissolution for basaltic glass measured in the laboratory to *in situ* conditions apparently leads to overestimate the rates of reaction. Chemically reactive surface area per volume of fluid is a critical parameter in this extrapolation and its value is dependent on the method used to measure it. Although it may not be the only explanation, the discrepancies can be caused by the presence of clays in conduits for fluid flow and as a replacement product of glass. Comparing our results with studies of Quaternary basalts in Iceland, the 10 Ma alteration history of the Mururoa basalt results in a decrease of the permeability of the aquifers by several orders of magnitude, but does not cause a large change of the chemically reactive surface area.

1. INTRODUCTION

A study of the chemistry of pore fluids in the volcanic basement of Mururoa atoll indicate that although most of the secondary phases precipitated earlier and at higher temperatures (60–120°C) (Dudoignon et al., 1989; Destrigneville et al., 1991), the alteration of volcanic glass and precipitation of secondary minerals (clays and zeolites) is continuing at the present low temperature (25–40°C) (Guy et al., 1992). Although the system is rock-dominated, there is little doubt that the interstitial fluid sampled in the volcanic basement was originally seawater and the increase of the rock/water ratio with depth and with the distance to edge of the atoll suggests that the system is open to a slow circulation of interstitial water towards the center of the atoll (Guy et al., 1992). We investigate thermal convection as a possible mechanism driving this flow.

There is a constant temperature difference between Pacific intermediate waters (4°C at 1000 m water depth) and the central part of the atoll heated by the geothermal flux (30–40°C at the same depth). This configuration is unconditionally unstable and buoyancy driven convection should occur at any nonzero permeability, unless the effect of the temperature difference is balanced by a salinity difference. As permeability tends to zero, fluid velocity also tends to zero, but no Rayleigh criterion applies to this mode of convection. The persistence of thermal convection even after the end of volcanic activity and cooling of the magma chamber may be quite general in atolls and should influence the alteration of the basement. Furthermore, geothermal upwelling within atolls has been proposed as a way to pump nutrient-rich intermediate or deep waters into the lagoon and maintain a high biological activity in some lagoons (Rougerie and Wauthy, 1993). The thermal convection models presented here provide a first order estimate of the water fluxes that can be expected from this thermal endo-upwelling, but the main objectives of this study are to constrain the average permeability of the basalts at atoll scale and to estimate the natural residence time of the pore fluid.

The rock-water ratio determined from chemical budgets and strontium isotope ratios varies from 20 to 150 grams of dissolved basalt per liter of porewater (Guy et al., 1992). In order to estimate the age of the fluid from these rock-water ratios, we extrapolate to natural basalt the reaction velocities measured in the laboratory on artificial basaltic glass samples (Guy and Schott, 1989). A similar approach has been applied to cold water aquifers in Iceland (Gislason and Eugster, 1987) and showed that the amount of basalt dissolved is related to the permeability and specific surface of the aquifer. However, the geologic setting in Iceland is very different from that in Mururoa. The water is fresh rather than saline, the basalt is tholeitic rather than alkaline (Maury et al., 1992), and the lavas flows are Quaternary in Iceland but are about 10 Ma old in Mururoa (Gillot et al., 1992). Due to this age difference, the alteration of the rock is more advanced in Mururoa (Gillot et al., 1992). Due to this age difference, the alteration of the rock is more advanced in

* *Present address:* ENS, Laboratoire de Géologie, 24 rue Lhomond, 75231 Paris Cedex 05, France.

Mururoa, with consequences on the permeability and presumably also on the reactive surface area. In Iceland, cold water flows mainly along a contact between subglacial hyaloclastites and postglacial aerial lava flows where permeability is very high, of the order of 1 cm/s (corresponding to about 10^{-9} m^2), but lower permeabilities are expected for Mururoa atoll.

We use the finite element method to model thermal convection in a two-dimensional cross-section of the Mururoa atoll. The confrontation of modeling results with temperature data helps to constrain the maximum permeability of the volcanic aquifers and confirms that it is several orders of magnitude lower than in Iceland. The uncertainty on the *in situ* reaction rate does not constrain the residence time of the fluid on the basis of the chemical model alone, but the combination of the thermal and the chemical models defines a range of possible values for the permeability and specific surface at atoll scale. Independently, porous media models, derived from Kozeny-Carman's model, provide relationships between permeability and specific surface that we compare to the finite element modeling results. Finally, the comparison of the Iceland and Mururoa cases gives indications on the evolution of the reactive surface area over long periods of time, which we discuss.

2. GEOLOGICAL SETTING

Mururoa atoll and its neighbour Fangataufa belong to a string of volcanic islands, comprising the Gambier Islands, the Duke of Gloucester's Islands, and at the eastern end, Pitcairn. These islands lay along the track of a hotspot which current location probably coincides with Pitcairn. The geology of the uppermost 600 m of the volcanic basement of Mururoa is well known from a number of boreholes drilled by the Commissariat à l'Energie Atomique (Buigues et al., 1992) (Fig. 1). Under the lagoon, reefal limestones and dolomites lie directly on the volcanic formations. Under the reef crown of the atoll, detrital sediments (muds and conglomerates) interlayered with carbonate strata form a transition zone. This zone is no thicker than 50 m, except in a few buried valleys, where it can reach more than 100 m. The depth of the base of the carbonate section is well constrained from drill hole data and surveys of the external slopes.

The upper part of the basalts, down to a depth of 500–600 m below present sealevel is mostly aerial lava flows. Submarine pillow-lavas and hyaloclastites form the lowermost section. Explosive events occurred as seawater was brought in contact with lavas at shallow depths. These events formed most of the subaerial volcanic rock unit in the central part of the volcano. Because of differences in the cooling rate of the lavas, aerial and submarine flows have a very different microstructure. The mesostase is mostly glass in submarine flows but is mostly microcristaline in aerial flows.

Radiometric K-Ar ages obtained in these formations cluster within a narrow time interval, between 10.7 and 11.8 Ma (Gillot et al., 1992). The lavas are an almost complete moderately alkaline series. Both endmembers types of lava (oceanite and trachyte) are found, but moderately differentiated terms (basalt and hawaite) dominate (Maury et al., 1992). Furthermore, the magmatic source appears to be isotopically homogeneous. All of these characteristics made it a good reference for the modelling of fractional crystallization (Caroff et al., 1992).

In spite of the chemical homogeneity of the lavas, their degree of alteration is highly variable. In massive submarine lava flows, the alteration is limited to olivine and vesicular glass. This alteration was modelled as tiny closed systems, in which the fluid is of magmatic origin (Destrigneville et al., 1991). Higher up in the pile, circulation of seawater and possibly meteoric water (in the aerial section of the volcanics) caused dissolution of glass, which was replaced by clay minerals (Fe-Mg Saponites and Chlorite-Saponite mixed layers). The alteration front progressed outward from veins and vesicles. In general, plagioclases are fresh and pyroxenes are altered very little. Vesicles and veins fill first with clays of similar chemical composition as those replacing the glass, then with zeolites (Dudoignon et al., 1989). The temperature at which these clays precipitated fall in the range of 60–100°C, based on measurements of oxygen isotopes ratios (Destrigneville, 1989). Because of the nature of the mineral assemblages and of their temperature of formation, most of the alteration has been considered to take place during the last phases of the cooling of the lava flows (Dudoignon et al., 1989; Destrigneville, 1989).

3. BOREHOLE DATA

3.1. Temperature Data

Vertical temperature gradients measured between 300 and 1000 m depth in the basaltic formations below the lagoon are well-clustered and there is no large systematic variation with the location of the drill holes. The average over logging profiles taken after thermal re-equilibration of forty-nine holes is 18.7 ± 3.2°C/km. For a thermal conductivity of 2.5 $W \cdot K^{-1} \cdot m^{-1}$ (Hyndmann and Von Herzen, 1977) the corresponding heat flow is 47 mW/m^2. However, these logging profiles were obtained in holes of large diameter (1.6 m), which unfortunately are subject to thermal convection. The resulting stratification can be seen in the staircase shape of some temperature profiles, and make gradient determinations imprecise, with a bias toward lower values. A few temperature logging profiles were obtained in normal diameter drill holes, but these are not always well equilibrated. The 3 profiles selected on Fig. 2 are ±1.5°C, corresponding to a ±6°C/km maximum error on the gradient. In the two holes drilled from the southern reef, the gradient in the volcanics is 31 and 24°C/km, while in the one drilled from the lagoon it is 28°C/km (see location on Fig. 1). We conclude that the geothermal heat flow is uniform in the volcanic basement.

Vertical temperature gradients in the carbonates is inverted on the logging profiles in all boreholes, and the minimum temperature is in general reached at the carbonate basalt interface (Fig. 2). That can be explained by a lateral input of cold water from the ocean. Many of the logging profiles obtained in large drill holes after thermal equilibration show steps of several °C near the base of the carbonates, indicative of fluid flow into the well. The temperature and salinity of water sampled at these levels are the same as at the same depth in the ocean.

3.2. Permeability

Fluid flow in the carbonates is dominated by a karst system. Dissolution cavities formed during the periods of low sealevel are horizontally connected with the ocean at different levels from the surface to at least 280 m depth. In the vicinity of the Exocet drill hole meter size caves were found in the massive dolomites near the contact with the basalts, at the same level where fluid flow into the wells was observed. The permeability of these open conduits are difficult to measure by standard pumping tests, but we can estimate that they are higher than 100 D.

Permeability measured on basalt samples varies in the range from 0.005 to 2 mD (Table 1). But this is not represen-

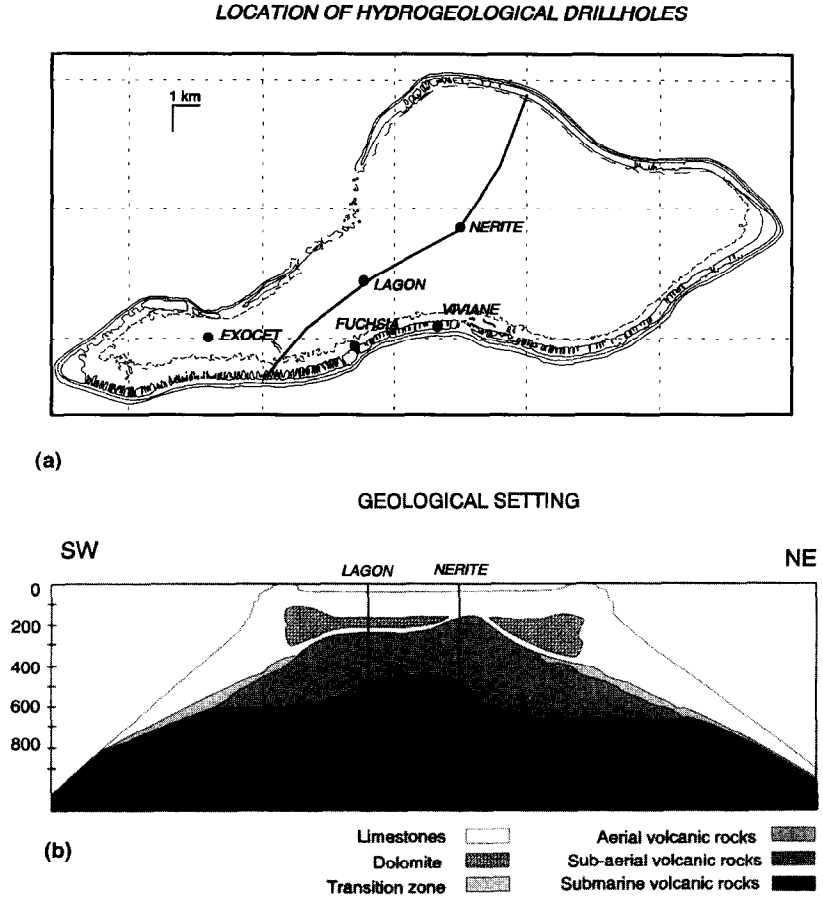

FIG. 1. (a) Map of Mururoa atoll showing the location of the studied drill holes and of cross-section in Fig. 1b. The interstitial water samples where taken using a packer device in Exocet and Nerite holes. Basalt samples studied for determination of the exchange surface are from Fuchsia drill hole. Temperature logging data from holes Fuchsia, Viviane, and Lagon are shown in Fig. 3. (b) Geological cross-section after Buigues et al. (1992).

tative of the permeability of the volcanic formations at the 10 m scale, and more probably, the permeability of aquifers should be used in the model. Pumping tests performed in the drill holes give permeabilities comprised between 0.1 mD and a few 100 mD (Fig. 3). A permeability of 0.1 mD Darcy corresponds to the lowest value measurable by this method. In Exocet the average permeability is about 100 mD in the interval where the pore fluid was sampled. In Nerite two aquifers having a permeability of about 10 mD are separated by a 20 m thick impermeable layer.

4. STRONTIUM CONCENTRATION AND WATER/ROCK RATIO

4.1. Principle of Rock/Water Ratio Determination

The rock/water ratio (R/W) defined as the mass of rock dissolved in one liter of water was determined from the strontium isotope ratio, assuming that strontium is not incorporated in the secondary phases (Guy et al., 1992). The initial strontium concentration in the fluid and the $^{87}Sr/^{86}Sr$ ratio are that of seawater: respectively, 8 ppm and $^{87}Sr/^{86}Sr = 0.709$. In the basalt, $^{87}Sr/^{86}Sr = 0.703$ and the concentration of Sr in the rock is taken equal to 800 ppm. The method used and results obtained are discussed in more detail by Guy et al. (1992), but we here precise its limitations on two points.

First, the concentration of Sr in the bulk rock may differ from that in the dissolved fraction. Plagioclases, which are not altered, tend to concentrate the Sr with a partition coefficient of 2 to 4 with respect to the melt (Caroff et al., 1992). Samples of submarine and aerial lavas were studied with a backscattering electron microscope and a microprobe. The sample of submarine basalt contains 50–70% glass and the rest is mostly plagioclase. Strontium content is 500 ppm in the glass and 1600 ppm in the plagioclase, which makes a bulk concentration of 830–1050 ppm. One cannot generalise from data on just one sample, although it is thought to be representative. But this result means that the R/W is probably underestimated, but certainly less than by a factor of two in the submarine basalts. In the aerial basalt sample we will assume that the bulk composition of the mesostase is about the same as that of the glass in the submarine sample.

Second, calcic zeolites, notably chabazite (Robert and Goffé, 1988), can take Sr. Thermodynamic models predict their precipitation for a high progress of the dissolution reaction but determinations of the R/W ratio at which they should

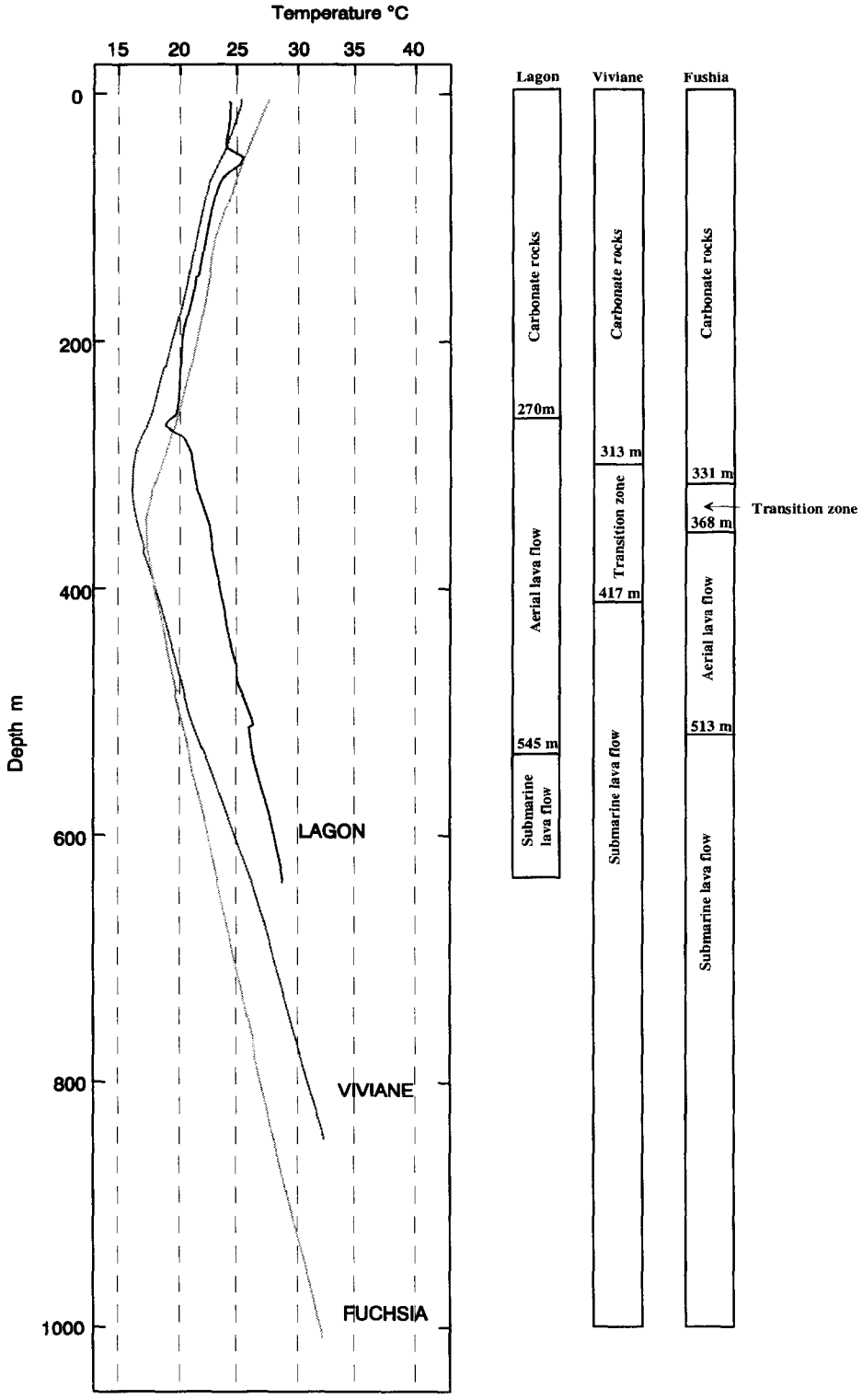

FIG. 2. Temperature logging profiles showing the temperature inversion in the carbonate section. Depth of the minimum temperature correlates with the top of the volcanic basement.

start to form are variable (Crovisier et al., 1992; Guy et al., 1992). However, the assumption that Sr is not removed from solution can be checked by comparing predicted and observed Sr concentrations. Results are concordant for concentrations of up to 50 ppm corresponding to R/W = 50 g/L (Fig. 3). But a gap (R/W = 110 g/L from isotope ratios

TABLE 1. Measured permeabilities and specific surface areas determined by Kozeny-Carman's law.

Porosity (%)	Permeability (m^2)	Specific surface area ($m^2 l^{-1}$)	observations
3.1	$6\ 10^{-18}$	$3.2\ 10^4$	submarine basalt
9.5	$5\ 10^{-18}$	$6.1\ 10^4$	submarine basalt
20.3	$1.8\ 10^{-15}$	$4.7\ 10^3$	submarine basalt
20-30	$5\ 10^{-17}$	$2.8\ 10^4$ - $3.5\ 10^5$	submarine basalt
25	$2\ 10^{-17}$	$5\ 10^4$	submarine basalt
30.1	1.9 10-15	$5.6\ 10^3$	submarine basalt
37	$8\ 10^{-17}$	$3\ 10^4$	aerial basalt

vs. 77 g/L from concentration) does exist in the deepest part of Nerite, where precipitation of calcic zeolites has occurred. In this case, the *R/W* ratios estimated by both methods bracket the actual value.

4.2. Field Data

The interstitial fluid was sampled at different depths in two drill holes, Nerite and Exocet (Fig. 4). Nerite is located near the summit of the buried volcano, while Exocet is located in the southwest part of the lagoon where carbonates lie on a subhorizontal lava platform at about 270 m below sea level.

In Exocet hole, a variety of facies is observed over a 90 m thick subaerial sequence (593–683 m), laying between typical submarine and aerial facies: hyalotuffs, heavily altered brechiated layers as well as more massive lava flows, and several limestone beds up to 10 m thick. In spite of this diversity, the chemical composition of the sampled interstitial water follows a very progressive trend, with rock-water ratio increasing from 20 g/L in the top of the section to 50 g/L in the bottom (Guy et al., 1992).

The Nerite hole is drilled in massive aerial lava flows, from 176 to 460 m below sealevel. Apart for a 50 m thick more altered interval which includes a brecchia layer, the formation is fairly homogeneous. Fluids sampled in the aqui-

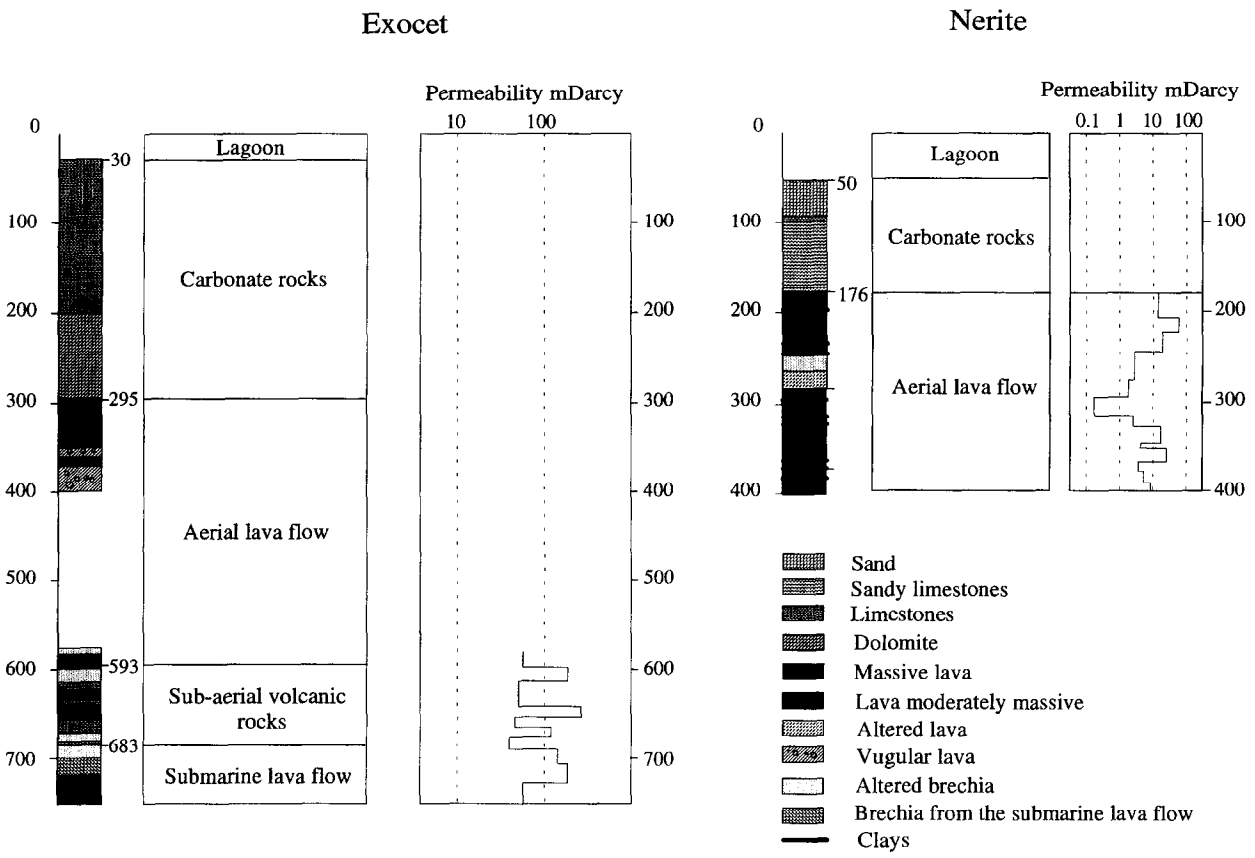

FIG. 3. Lithostratigraphy of Nerite and Exocet drill holes and permeability measurements from packer tests.

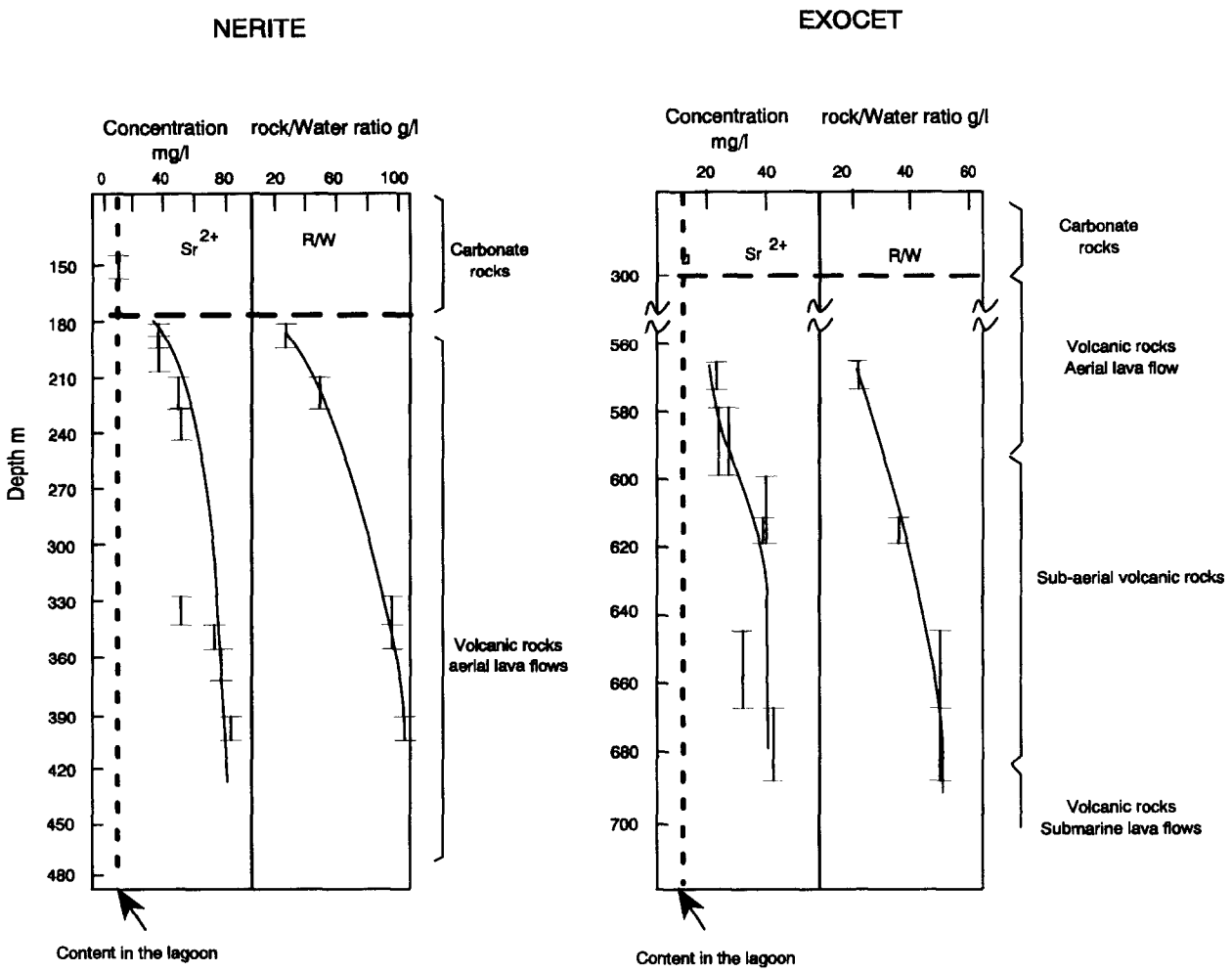

FIG. 4. Strontium concentration and estimates of rock-water ratio from strontium isotopic ratio in porewater from drill holes Exocet and Nerite, after Guy et al. (1992).

fers also show a progressive trend with R/W ratio increasing from 20 g/L at the top of the volcanic formations to about 100 g/L at 400 m depth. The higher R/W ratio in this hole may be related to the lower permeability of the aquifers compared to Exocet.

In each hole, lithological differences between strata seem to have little influence on the R/W ratio. This averaging out can be partly due to the use of a packer which isolates 10–20 m intervals for sampling.

5. ESTIMATION OF IN-SITU REACTION RATE

The R/W ratio is related to the time of residency τ of the interstitial water by:

$$R/W = S'_w \nu\tau, \quad (1)$$

where S'_w is the chemically reactive surface in contact with a liter of water and ν is the velocity of dissolution per unit surface. For submarine lava flows the active surface is essentially the glass-water interface, and ν is determined from laboratory experiments on synthetic glasses of basaltic composition. We will assume that the rate of dissolution is the same in the aerial volcanism.

5.1. Basaltic Glass Dissolution

Dissolution kinetics of basaltic glass were measured under a wide range of temperature (25–300°C) and pH (2–10) in open and closed system (Berger et al., 1987; Guy and Schott, 1989; Crovisier et al., 1987). These experiments enabled us to determine the different mechanisms during the dissolution. At low temperature, surface reaction controls the bulk dissolution; diffusion of ions in the solution and through an altered layer do not reduce the leaching rate. Furthermore, it has been shown that the presence of silica and aluminium in the solution induces a decrease of the dissolution kinetic (Berger et al., 1994). This behaviour can be understood within the frame work of the transition state theory which predict that dissolution and precipitation kinetic laws are proportional to the thermodynamic imbalance of the solution toward the reacting minerals (Aagaard and Helgeson, 1982). At equilibrium, minerals stop to dissolve or precipitate. As

basaltic glass is thermodynamically unstable, equilibrium is never reached. However, the concentration of leached elements in the solution causes the precipitation of secondary phases (clays such as smectites, Berger et al., 1987). In the solution, a stationary state is reached when the kinetics of glass dissolution and clay precipitation are equal. This stationary dissolution kinetic is characteristic of long-term alteration. Dissolution kinetics of basaltic glass at stationary state have been measured from 50 to 200°C in seawater type solution (Guy, 1989; Berger et al., 1994). They are about 500–1000 times lower than the initial dissolution rate measured in a silica-free solution. We have calculated at lower temperatures the dissolution rate from these experimental data using Arrhenius law and assuming an activation energy of the dissolution E_a = 60 kJ/mole (Guy and Schott, 1989):

$$\nu(T) = \nu(T_0)e^{Ea(1/RT_0 - 1/RT)}, \quad (2)$$

we obtain 2.5 10^{-3} $g \cdot m^{-2} \cdot a^{-1}$ at 25°C and 3.5 10^{-4} $g \cdot m^{-2} \cdot a^{-1}$ at 3°C. The latter value has been compared to the rate of palagonitization of submarine basalt calculated by Hekinian and Hoffert (1975) from the thickness and the rate of accumulation of manganese encrustation. Assuming a rate of Mn accumulation of 1–14 $\mu m/10^3$ y and using the linear correlation between the thickness of Mn and palagonite, they found a rate of palagonitization from 0.7 to 35 $\mu m/10^3$ years or 0.2 to 10 10^{-4} $g \cdot m^{-2} \cdot a^{-1}$.

5.2. Basalt Dissolution

In this study, dissolution of basalt have been performed at 90°C in pure water and seawater with Teflon closed reactors. Both unaltered aerial and submarine basalt were used in the experiments. A 100–150 μm fraction was separated by dry sieving. In order to remove adhering ultrafine particles, the ground material was treated by high-energy ultrasonification in acetone. Repeated treatments were necessary to dislodge all fine particles. The specific area of the powder, assuming spherical grains, was 160 cm^2/g. Dissolution rates have been measured from silica analysis, according to a previous study on the basaltic glass (Guy and Schott, 1989). The dissolution rates measured in free silicon seawater and in pure water are very close. Table 2 summarizes the dissolution rates of powders of basalt, basaltic glass, and basalt constitutive minerals (olivine, plagioclase, pyroxene) measured or calculated at 25°C from experiments conducted at higher temperature in free silicon solution (Grandstaff, 1980; Holdren and Berner, 1979; Schott et al., 1981). The dissolution rates of basalt measured at 90°C have been calculated at 25°C assuming an activation energy of the dissolution of 60 kJ/mole. The dissolution kinetics of both unaltered aerial or submarine basalt are lower than that of the basaltic glass by a factor of one-third to one-tenth and are always higher (more than one order of magnitude) than that of the different minerals. These data seem to show that the dissolution of basalt is controlled by the basaltic glass rather than by the constitutive minerals. Furthermore, numerous observations from sample sections show that pyroxene and plagioclase remain unaltered and that basaltic glass and olivine are always replaced by clays (Dudoignon et al., 1989; Destrigneville, 1989). From these results, we assumed that only the basaltic glass controls the composition of the solution dissolving the basalt and the dissolution kinetics of the basaltic glass characteristic of the long-term alteration were applied for both the aerial and submarine basalt.

TABLE 2. Rate of silica release at 25°C.

Minerals	Dissolution rate at 25°C in dilute solution mole.cm^{-2}.s^{-1}
Olivine:	
Forsterite	1.2 10^{-16} (1)
Plagioclase:	
Albite	1.19 10^{-15}(2)
Pyroxene:	
Enstatite	1.0 10^{-14} (3)
Diopside	1.4 10^{-14} (3)
Basaltic glass	3 10^{-13} (4)
Basalt	0.3 - 1 10^{-13} (5)

(1) Grandstaff (1980); (2) Holdren and Berner (1979); (3) Schott et al. (1981); (4) Guy and Schott (1989); (5) this study.

5.3. Laboratory Measurements of Specific Surface

Among the different methods that can be used to measure the specific surface of a laboratory sample (Scheidegger, 1972) we have tried three, with variable results.

5.3.1. Kozeny-Carman model

Specific surface can be estimated from permeability and porosity measurements, using a geometrical model of porous medium (Kozeny, 1927; Carman, 1937). This method is discussed in more detail in the section "specific surface and permeability at atoll scale." The underlying assumption is that the average radius of the pores and the specific surface are directly related. Thus it can be wrong if the surfaces are highly irregular with many asperities smaller than the pore radius and is also very sensitive to precipitation of clays in the pore space. Permeability and porosity are measured in the laboratory under in situ conditions of interstitial pressure and effective pressure. The total pore surface per pore volume S_w (Table 1) is computed with $a = 1/5$ and $f = 1$ (minimum tortuosity):

$$S_w = \sqrt{af\varphi/k}. \quad (3)$$

Permeability differs dramatically from 5 10^{-18} to 1.8 10^{-15} m^2. The high variability of permeability for samples of large porosity (20–30%) probably depends on the existence or absence of unclogged channels.

5.3.2. B.E.T. Method

The specific surface of the synthetic basaltic glass samples used in the dissolution experiment was measured by the B.E.T. (Brunauer-Emmet-Teller) gas adsorption method. It has also been tried on natural aerial basalt samples. Basalt and basaltic glass are first crushed. They are then sifted through brass sieves to separate the different powder fractions. Each fraction is rinsed ultrasonically in acetone. After

TABLE 3. Specific surface area determined by the B.E.T. method.

Sample	Powder size (μm)	Specific surface ($m^2.g^{-1}$)
synthetic glass 1, unaltered	100-125	0.045
synthetic glass 2, unaltered	135-350	0.018
synthetic glass 3, unaltered	135-360	0.031
synthetic glass 3, altered	135-360	0.1 - 1.6
natural basalt 1	whole sample	0.41
natural basalt 1	63-100	5.8
natural basalt 1	100-125	3.08
natural basalt 1	500-630	3.86
natural basalt 1	600-800	5.59
natural basalt 1	800-1000	5.13
natural basalt 2	100-315	18.4
natural basalt 3	100-315	11.7
natural basalt 4	100-315	1.44

rinsing with ultra pure water, all powders are dried for more than 72 h at 50–60°C. The specific surface is here expressed as a surface per mass of solid (Table 3). The results for unaltered synthetic glass powders are consistent with the size of the grains and the roughness defined as the deviation from the geometrical area for spherical grains varies from 2 to 5. Alteration of the synthetic glass increases the measured specific surface by a factor of 3–50. The specific surface is even higher for natural samples. The results on sample 1 shows that the specific surface does not vary when increasing the grain size from 63–1000 μm. Therefore, adsorption on internal surfaces is dominant. As the specific surface of clays ranges from 10–500 m^2/g (Neuzil, 1994), this behavior can be explained if only a small fraction of clays stays attached to the basalt particles or remains as aggregates. Indeed, the measured specific surface increases with the degree of alteration of the samples. (sample 4 is the least altered and samples 2 and 3 are the most altered). The massive sample has a specific surface about ten times lower than the powders. It is possible that the measurement time is not long enough to let the gas access to all poral space. In conclusion, the cleaning procedure has been inefficient in removing alteration products. For synthetic glass samples the large increase of specific surface may be due to alteration products rather than an increase of surface rugosity.

5.3.3. *Geometrical determination*

Geometrical determination of porosity and specific surface from random sample sections is possible with the assumption that the porous medium is statistically homogeneous and that the surface distribution is isotropic. Porosity φ is proportional to the surface of the pore on the cross section, and the specific surface of the pores is proportional to their perimeter (Weidel, 1980).

$$S_{spe} = \frac{4}{\pi} \frac{\sum_{\text{SECTION}} \text{perimeters}}{\text{section} \cdot \text{area}} \text{ and } \varphi = \frac{\sum_{\text{SECTION}} \text{pore} \cdot \text{area}}{\text{section} \cdot \text{area}}. \quad (4)$$

Two samples of submarine basalt and one sample of aerial basalt, from Fuchsia drill hole, were studied. One submarine basalt sample is very altered. Most of the glass has been replaced and the glass-water interaction surface is therefore very small. The other sample still has unaltered glass and the interface between glass and replacement products is easily identified both on optical microscope and backscattered electron S.E.M. (B.E.M.) images (Fig. 5). B.E.M. photographs were scanned with 256 grey levels and 768 × 512 pixels (the pixel size is then a few tens of a micron). After contrast enhancement, several filters are used (linear and nonlinear filters, Fourier transform) and a threshold is applied. The image is transformed in a binary image: each pixel is "pore" (actually meaning clays) or "not pore" (Fig. 6). Finally, the perimeter and the area of all pores is computed and the specific surface area and the porosity is determined. Note that in order to obtain the water content the porosity must be corrected for the presence of clays in the pores.

The surface covered by the B.E.M. mosaic is too small for a reliable specific surface measurement. However, we used it to estimate the rugosity of the surfaces with the following procedure. Glass and olivine alteration fronts where divided in segments 50 or 10 μm length, depending on the scale of the images. The length of the alteration front measured in pixels (of size 0.1–0.5 μm) is longer than the segment length by a factor of 1.5–3.3 for the glass, and of 2 to 9 for olivines. The existence of such a multiplicating factor when the scale of measurement is changed can be modelled as a fractal dimension D, defined as

$$\left(\frac{L}{L_0}\right) = \left(\frac{l_0}{l}\right)^{D-1}, \quad (5)$$

where L is the length of the line measured at the pixel size l and L_0 is the length measured with segments of length l_0. This fractal dimension varies from 1.11 to 1.18 for the glass. It is an average property of the surface over the range of scale from 100 to 0.1 μm. The corresponding length multiplicating factor for this scale change is 2.1 to 3.5. As far as Eqn. 4 is valid, the same multiplication factor applies to the perimeters and to the surfaces. For olivines, the rugosity of the surface is more variable, but we did not take the olivine-water interface into account.

The next step was to measure the length of the glass-water interface on the optical microscope mosaic by dividing it in 100 μm segments. Only surfaces which correspond to the glass alteration front where taken into account. For example,

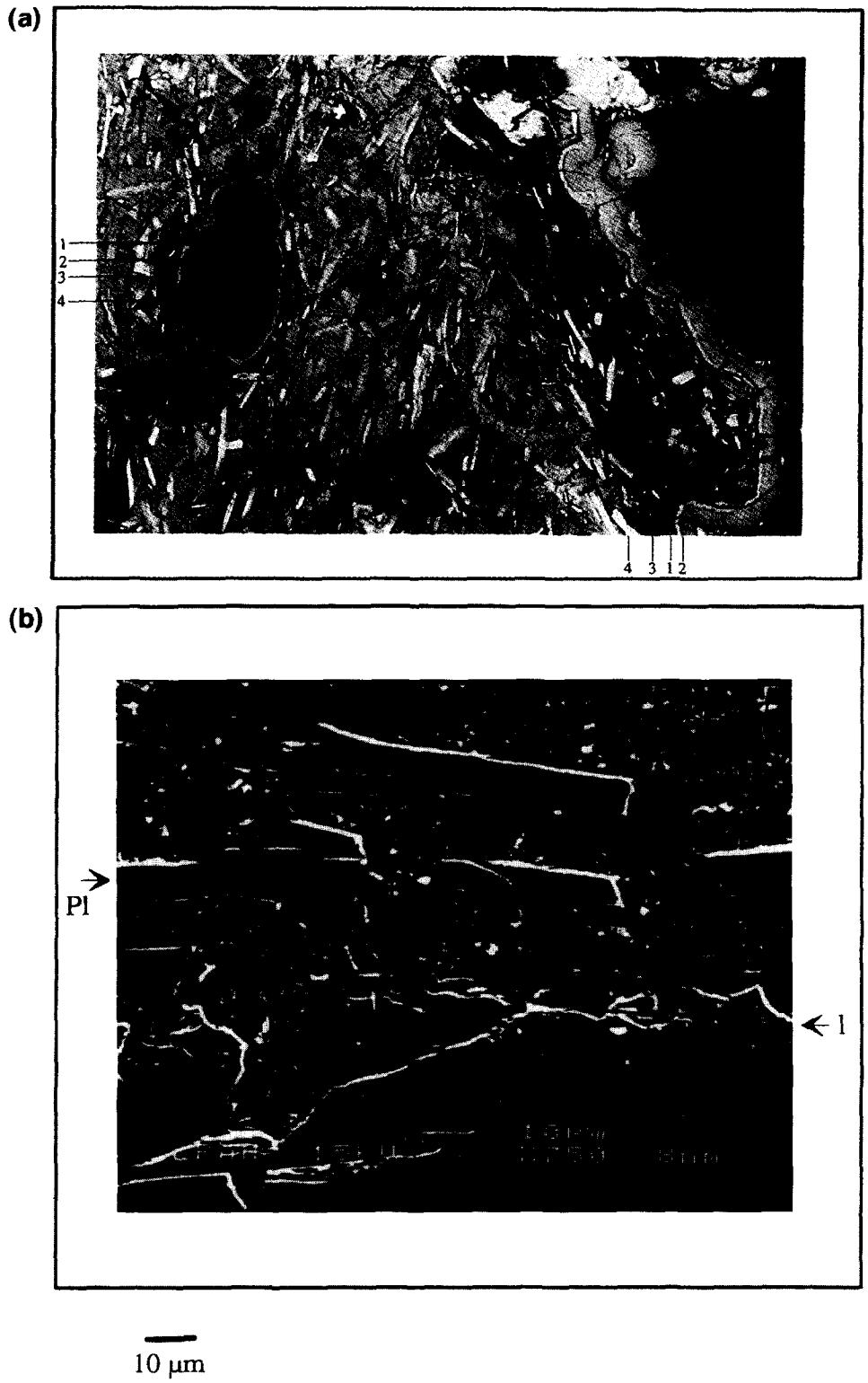

FIG. 5. Altered basalt from a submarine lava flow. (a) Thin section under natural light. Concentric precipitation in the vacuole and on the rim of the sample produced first a thin celadonite layer (1), followed by a Fe-Mg saponite layer (2). Glass replacement proceeds from the vacuole and the rim of the sample. Alteration products replacing the glass (mostly Fe-Mg saponites) form two layers: a darker one in contact with the celadonite layer (3) and a brighter one in contact with the glass (4). The limit between intact glass and alteration products is sharp and does not have a high rugosity at this scale. Plagioclase resists alteration and still occurs in the outer dark layers. (b) BEM image taken on the same sample. The limit (1) of glass alteration crosses the lower part of the image. Plagioclase rods (Pl) are seen in unaltered glass, where they appear darker, as well as in the clay matrix where they are well outlined by their brighter rim.

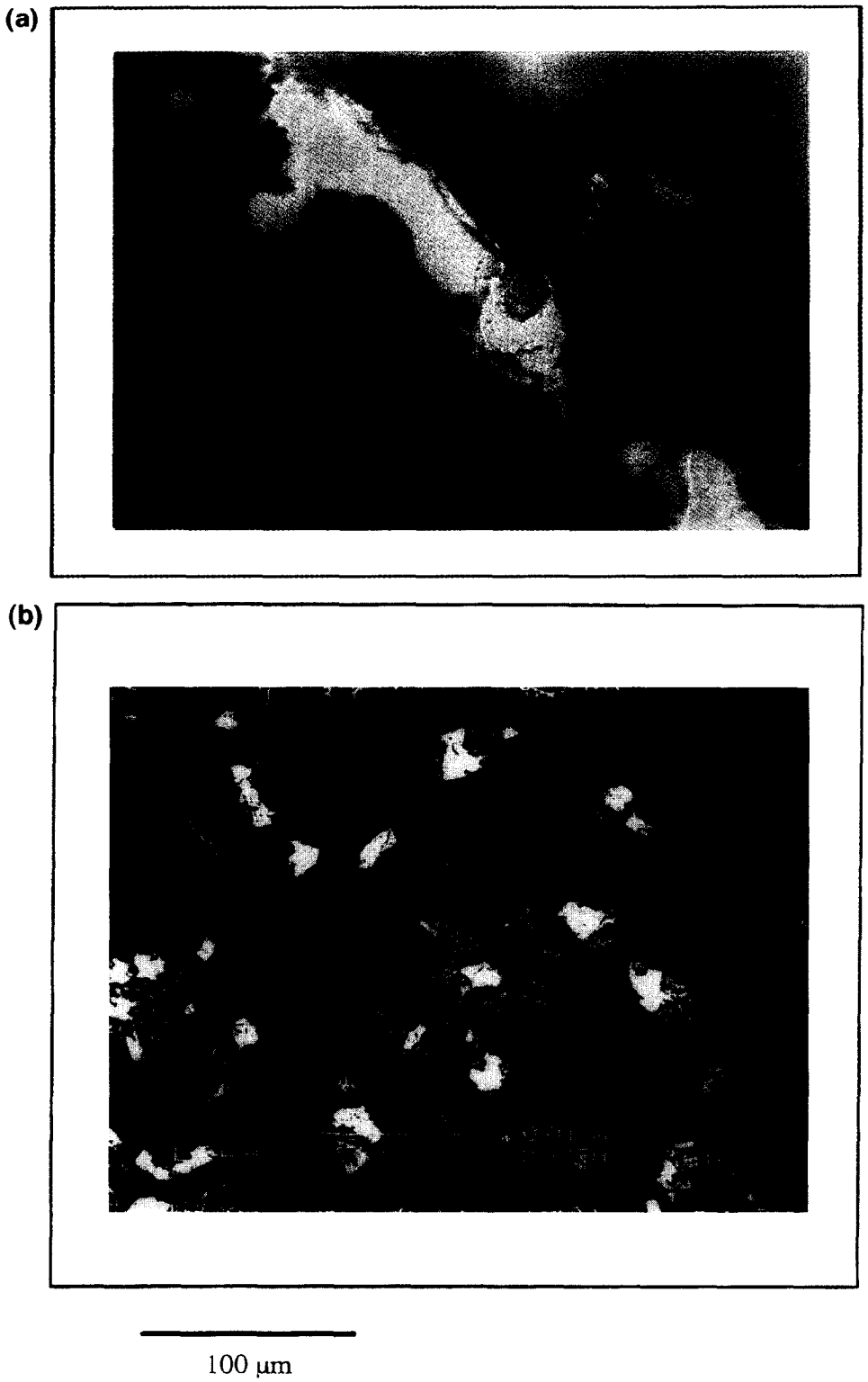

FIG. 6. Basalt from an aerial lava flow. (a) Fluorescence of UV light section. The sample has been impregnated with fluoresceine before cutting to show the connected porosity. The bright region is a fracture filled with clay. Although they do not appear to be connected in two dimensions, tiny pores in the surrounding rock, also filled with clay, are impregnated as well. (b) BEM image showing the micro crystalline structure and clay-filled micropores. A vein cuts the sample at the right end of the image. No surface was identified as glass. (c) Same image after processing. Pores are in black. The surfaces and perimeters of pores and the length of the vein wall can be easily measured on the image. Here, pore surface is about 10% of total image surface.

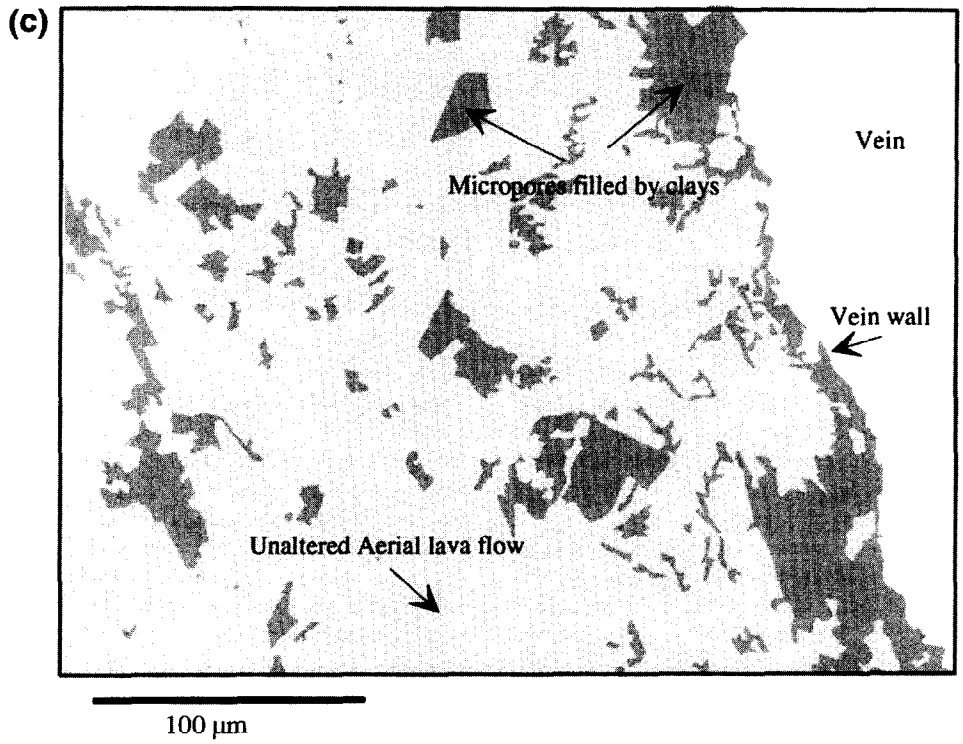

FIG. 6. (Continued)

small fractures with no visible glass alteration around them were discarded. For a sample surface of about 10 mm^2, the perimeter measured by two different observers is between 37 and 44 mm. The specific surface expressed as the surface per unit rock volume is 4.45–5.2 mm^{-1} at the 100 μm scale, and thus, should be between 9 and 18 mm^{-1} when extrapolated to the 0.1 μm scale. Assuming a water content of 10%, we obtain S'_w in the range 90–180 m^2/L.

The aerial basalt sample is almost completely crystallized but contains many tiny pores filled with clays. Impregnation with fluoresceine showed that these tiny pores are connected to the neighbouring veins (Fig. 6). We do not know whether these clay assemblages are late glass replacement at low temperature or are formed during the cooling. No glass was identified on the B.E.M. images. It implies that the glass fraction in this basalt is small rather than glass is absent. But we could not determine a reactive surface area for this material. The clay filled pores however can be easily identified and measured (Fig. 6b,c). The porosity away from the veins is 6% in average but increases near the vein, indicating alteration of the microcristals in the mesostasis.

5.3.4. Implications for the in situ reaction rate

The comparison of the specific surface areas in Table 4 emphasizes the difficulties in determining accurately this parameter in a partially altered rock, as it is both dependent on the method used and on the scale at which it is measured. Except for the Kozeny-Carman method, when it is applied to samples for which the porosity is known, the estimates are made assuming an average porosity of 10%. Direct estimates from optical and B.E.M. images are much lower than results of the two other methods. Measurements on B.E.M. images showed that for a change of measuring scale from 100 to 0.1 μm the surface of the glass alteration front is only increased by a factor of 2.1–3.5 (corresponding to a fractal dimension of 2.11–2.18). The measurement scale for the B.E.T. method is a few nm, which is another jump by a factor 1000. It would be very surprising if this surface would be increased by a factor of 100–1000 over this range (corresponding to a fractal dimension of 2.67–3). The geometrical measurement on sample cross-sections is probably the best way to estimate the specific surface, as it enables to identify the various surfaces, and to measure only chemically reactive surfaces. Among the three samples, one has a fairly high glass dissolution surface, while the two others have none because of the lack of glass. For this reason, generalization from thin sections to rock formation scale would require a larger number of samples.

Assuming S'_w = 100 m^2/L for a porosity of 10%, and a rate of glass dissolution ν = 2.5 10^{-3} $g \cdot m^{-2} \cdot a^{-1}$ at 25°C, the rate of increase of the R/W ratio of the pore fluid is 0.25 $g \cdot L^{-1} \cdot a^{-1}$. With this value, the highest measured R/W ratios are obtained in less than 1000 y. With the same parameters and for a bulk rock density of 2700 kg/m^3, the rate of alteration of the basalt is 10^{-5} a^{-1}. This means a total alteration of the rock in 100.000 a. As the age of the basalts is 10 Ma, this reaction rate is obviously too high. If the surficial reaction rate is correct, then the average reactive surface should be very low to be compatible with the presence of still unaltered glass: S'_w = 1 m^2/L. Furthermore, we will show in the following section that a residence time of the order of 1000 years for the interstitial fluid is incompati-

TABLE 4. Comparison of specific surface areas determined by different methods, assuming 10% average porosity.

Method	Surface area per fluid volume S_W (m^2l^{-1})	Observations
B.E.T.	2.10^4 - 2.10^5	aerial basalt, probably with clays
Kozeny - Carman	5.6 10^3- 6.1 10^4 (sample scale) 450-1400 (atoll scale)	aerial and submarine basalt
Optical microscope & B.E.M	90-180	glass reactive surface in submarine basalt

ble with the thermal structure of the basement. Assuming $S'_w = 1$ m^2/L, the times of residency are from 8,000 to 20,000 years in Exocet hole, and in the upper aquifer in Nerite hole (180–240 m depth), and about 40,000 years in the lower aquifer (330–400 m depth).

The discrepancy between the age of the basaltic formation and the estimated reaction rate may be explained by the heterogeneity of alteration. In altered zones, reaction rate is expected to drop as glass is removed and in fresh massive basalt, reaction rate should be very low as water is not available. At a given time, alteration may only occur in a part of the formation but fluids should interact with rocks at various stages of alteration as they migrate through the formation. We will assume the chemistry of the interstitial fluid reflects interaction with an average rock, representative of the aquifer.

6. THERMAL CONVECTION MODEL

6.1. Equations Solved by the Finite Element Model

The Métis finite element program was developed by P. Goblet at the Ecole des Mines de Paris. This program uses a standard Galerkin formulation and solves problems of thermal convection in porous media and of transport of chemical tracers. For cases involving buoyancy driven convection, the heat transfer equation

$$\nabla((\Lambda + \bar{\alpha}\,|U_D|\rho c_w)\nabla T) - \rho c_w U_D \cdot \nabla T = \rho c \frac{\partial T}{\partial t} \quad (6)$$

and the fluid flow equation

$$U_D = -\frac{k}{\mu}(\nabla P - \rho g) \quad (7)$$

are solved sequentially at teach time step. Symbol definition is given in Table 5. Following Bousinesq's approximation, the fluid is considered to be incompressible, except for the computation of the gravity term which couples the two equations.

The density of the fluid is approximated with a linear temperature dependence but salinity variations are not taken into account. Variations of salinity do occur. In Exocet hole, precipitation of clays which contain 10–16% water result in an increase in chloride concentration from 560 to 600 mM and in salinity up to 40.5 g/L (Guy et al., 1992). However, this trend of increasing salinity probably stops at higher rock-water ratios: in Nerite hole recrystallization of clays releases water and maintains chlorinity between 554 and 580 mM. This effect combined with exchange of Na + Ca for Mg result in a slight decrease of salinity, down to 32.4 g/L (Guy et al., 1992). Corresponding extreme variations of density with respect to seawater (salinity 35 g/L) are +3.5 and −1.8 g/m^3. The density variation due to the 20–30°C temperature difference between the central part of the atoll and ocean intermediate waters are −5 g/m^3 to −8 g/m^3. The effect of the salinity variations on fluid density, although not negligible, appears to be smaller than the effect of the temperature variations. Because salinity variations may oppose or favor convection depending on the progress of the alteration reaction, their impact is difficult to estimate.

6.2. Model Geometry and Physical Parameters

We have chosen to model a N–S section across the western part of the atoll, on which the Exocet drill hole is located (Fig. 2). Only two petrological domains are defined: volcanic basement and carbonate section.

Homogenous physical parameters are used for each of the two domains. Average thermal capacity is computed with a porosity of 30% in the carbonates and of 10% in the basalts from the thermal capacity of water and from an average value for minerals (Table 5). Typical thermal conductivity values are used for carbonates and basalt (Hyndmann and Von Herzen, 1977; Brigaud, 1989). Unlike permeability and chemical reaction rates, thermal conductivity and heat capacity are not subject to large variations from one strata to another and changing their values within the acceptable range would have little influence on the results.

As the bulk permeability of the carbonates section is unknown, we use the convection model to estimate its probable range. The influence of this parameter on the fluid circulation in the basement is small.

The average permeabilities of the formations in which the fluid where sampled is about 100 mD in Exocet, and about 10 mD in Nerite. These values agree with measurements from packer tests in ODP drill holes in young oceanic upper crust (Becker et al., 1994). Two models, with constant intrinsic permeabilities of 10^{-14} m^2 and 10^{-13} m^2, corresponding, respectively, to about 10 mD and 100 mD are tested. Much lower permeabilities have been measured in Nerite, but are probably not representative of the aquifers where the fluid flow takes place. We will show that the modeling results

TABLE 5. Parameters of the thermal convection model.

A: Heat transfer equation

Symbol	Definition	Formula	Numerical values
T	temperature		
φ	total porosity		carbonates: 30% basalt: 10%
ρc_w	water volumetric heat capacity		4 10^6 J/m^3°K
ρc_g	minerals volumetric heat capacity		~2.2 10^6 J/m^3°K
ρc	bulk volumetric heat capacity	$\varphi\rho c_w + (1-\varphi)\rho c_g$	carbonates: 2.8 10^6 J/m^3°K basalt: 2.4 10^6 J/m^3°K
Λ	thermal conductivity		carbonates: 2 W.m^{-1}.K^{-1} basalt: 2.5 W.m^{-1}.K^{-1}
$\bar{\bar{\alpha}}$	dispersivity tensor	$\begin{pmatrix}\alpha_L & \alpha_T \\ \alpha_T & \alpha_L\end{pmatrix}$	α_L = 10 m α_T = 1 m
Pe	Péclet number (thermal)	$\frac{\rho c_w L.U_D}{\Lambda}$	L, fluid path length, is typically 1 km

B: Darcy equation

Symbol	Definition	Formula	Numerical values
U_D	Darcy velocity		
P	fluid pressure		
g	gravity		9.81 m.s^{-2}
ρ	fluid density	$\rho = \rho_0(1-\beta(T-T_0))$	ρ_0 = 1020 kg/m^3 β = 2.6 10^{-4} K^{-1} T_0 = 25°C
k	permeability		carbonates: 3 10^{-11} m^2 basalt: 10^{-13} to 10^{-14} m^2
μ	fluid viscosity		approximated by that of pure water (10% error)

can be extrapolated to smaller permeabilities from the linear properties of the equations, and that smaller average permeabilities do not give satisfactory results. The available data do not provide enough constrains to propose a more complex model of the atoll.

6.3. Boundary Conditions

Temperature and pressure are fixed on the bottom of the lagoon and in the ocean. Seasonal and tidal variations are not taken into account. In the model, the seasonal variations of the temperature and salinity of the surface waters should not influence the convection in the basalts because the recharge occurs at the level of intermediate waters. The amplitude of ocean tides is less than 1 m between high and low tide, implying that the maximum pressure difference between the ocean and the interior of the volcanic basement is 5×10^3 Pa. This is one order of magnitude lower than the pressure difference driving the convection in the basement (about 5×10^4 Pa at 1 km depth for a density difference of 5 g/m^3). Flows induced by tides are described as a diffusion process (Fang et al., 1993). Using their formulation, the maximum value for the characteristic depth of penetration for the tidal flux is estimated to about 150 m (assuming a permeability of 10^{-13} m^2, a fluid viscosity of 10^{-3} Pa.s, and a specific storage of 5×10^{-11} Pa^{-1}), which is small compared to the length of the modelled cross-section. Furthermore, these tidal fluxes should cancel out in average. For these reasons the temperature field in the volcanic basement should not be affected by the tidal flows and the steady-state thermal convection flow can be computed with average boundary conditions. Thus, the temperature at the boundaries is taken from the average of measured values. It decreases from 26°C at the surface and in the lagoon, to 4°C at 1200 m depth at the base of the section used for the model. Pressure is computed by integration of the density over the water column. Salinity variations are not taken into account.

In agreement with the measurements and with the 40–50 Ma age of the oceanic crust surrounding the islands, the value retained for the heat flow through the base of the model is 50 mW/m^2.

Finally, the lower limit at 1200 m below sea level is assumed to be impermeable, arbitrarily limiting the base of the convection cell. As indicated by the increase of W/R with depth and by the trend of alteration effects, the water-rock system tends to be less open as one goes deeper in the basement. It may be risky to extrapolate below the base of the drill holes, but the observations suggest that convection fades with depth.

6.4. Initial State and Evolution Towards a Steady state

The model runs in transient state. The initial state was arbitrarily set to the steady state in the absence of fluid movement. The geothermal flux keeps the inside of the island at a higher temperature than the slopes, which equilibrate with the ocean (Fig. 7). This situation is unstable for any value of the Rayleigh number of the system. In the first few hundreds of years, cold seawater invades the carbonates, causing a temperature inversion. Consequently, thermal convection in the carbonates slows down by a factor of 10

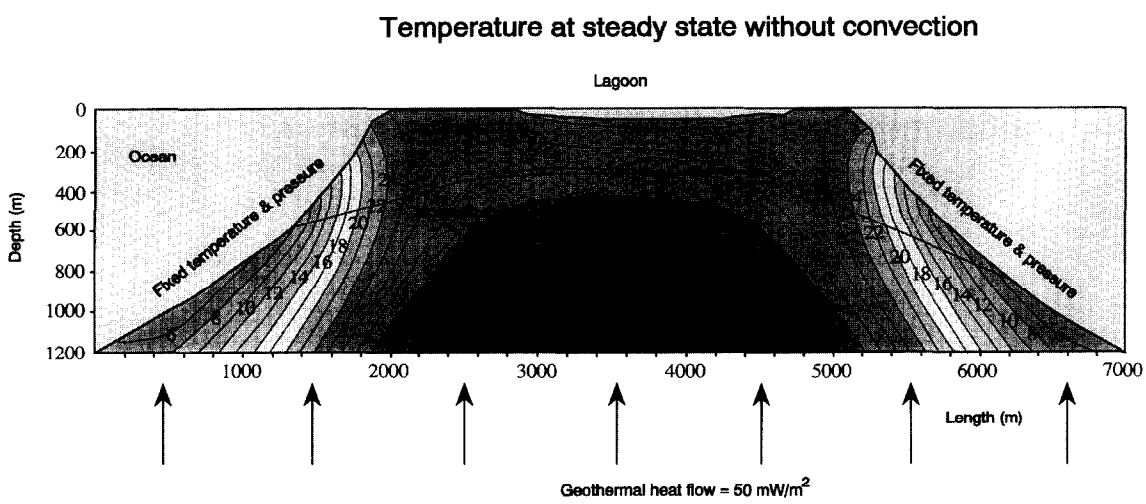

FIG. 7. Boundary conditions of the thermal convection model and computed temperature field in the absence of water convection.

or more. The volcanic basement then cools, essentially by conduction from the top. The geometry and the velocity of flow changes little during this second phase. A steady state is reached in roughly 100,000 years, but this value is very dependant on the thickness of the basalt layer included in the model.

6.5. Thermal Convection in the Carbonate Section: Modeling Results

The same modeling approach as in this study has already been applied to the carbonate (Samaden et al., 1985). Cold water enters horizontally through the sides, warms up, and is expelled upward into the lagoon (Fig. 8). This geothermal upwelling within the carbonates has been proposed as a way to pump nutrient-rich intermediate or deep waters into the lagoon and maintain a high biological activity in some lagoons and possibly help the growth of coral reefs on the ocean side (Rougerie and Wauthy, 1993). However, studies in atoll and lagoon hydrology suggest that ocean tides may be more efficient for the mixing of water within the highly permeable carbonate formations. For example, the role of tides in mixing seawater and freshwater lenses was established for Enewetak atoll (Herman et al., 1986; Oberdorfer et al., 1990) and differences in water level between ocean and lagoon also can be a significant driving force (e.g., Join et al., 1988). In the thermal convection model, a bulk permeability of about 30 Darcy is needed to reproduce the measured temperature profiles (Fig. 9). The corresponding water flux is about 300 m^3/a for the modelled atoll cross-section, or about 10^7 m^3/a for the whole atoll. In the carbonate formations fluid flow probably occurs mostly through karstic conduits and may not follow Darcy's law. The permeability value determined here should only be considered as a lower bound. The temperature field computed with the model fits the measurements and thus provides a good upper boundary condition for the volcanic basement on which we concentrate in this study.

6.6. Thermal Convection in the Volcanic Basement: Modeling Results

Fluid flow in the basement follows the same pattern as in the carbonate section but is much slower (Fig. 8). For a permeability of 10^{-14} m^2, the Darcy velocities are of a few millimeters per year (10^{-10} m/s) only (Fig. 10). The corresponding thermal Peclet number is about 0.1 for a 1 km typical path length, which implies that the water flow is too low to significantly change the temperature field (Fig. 9). Therefore, for uniform permeabilities lower than 10^{-14} m^2 the variation of the flow velocity with the permeability is linear. If the permeability is increased to 10^{-13} m^2, Darcy velocity increases by one order of magnitude, to a few centimeters per year (10^{-9} m/s). The Peclet number is then about 1 for a 1 km path length and the volcanic basement is cooled by the convection. In this case, the value of the temperature gradient near the interface with the carbonates decreases away from the center and drops to almost zero under the reefs. The temperature gradient in the uppermost volcanics does drop to low values in a few of the boreholes drilled from the reef crown, but not in the vicinity of the modelled cross-section. As this cooling is not a frequent feature, the average permeability of the volcanic formations should be lower than 10^{-13} m^2. As pointed out by Fisher and Becker (1995) in a mid-ocean ridge context, closed cell supercritical Rayleigh convection should occur in very permeable aquifers (10^{-9} or 10^{-10} m^2), even if they are not connected to the seafloor, but the existence of such a fast convection would also cause large lateral heat flow variations, which are not observed.

With an average porosity of 10%, the average velocity of the fluid is 10 times the Darcy velocity. For a path length

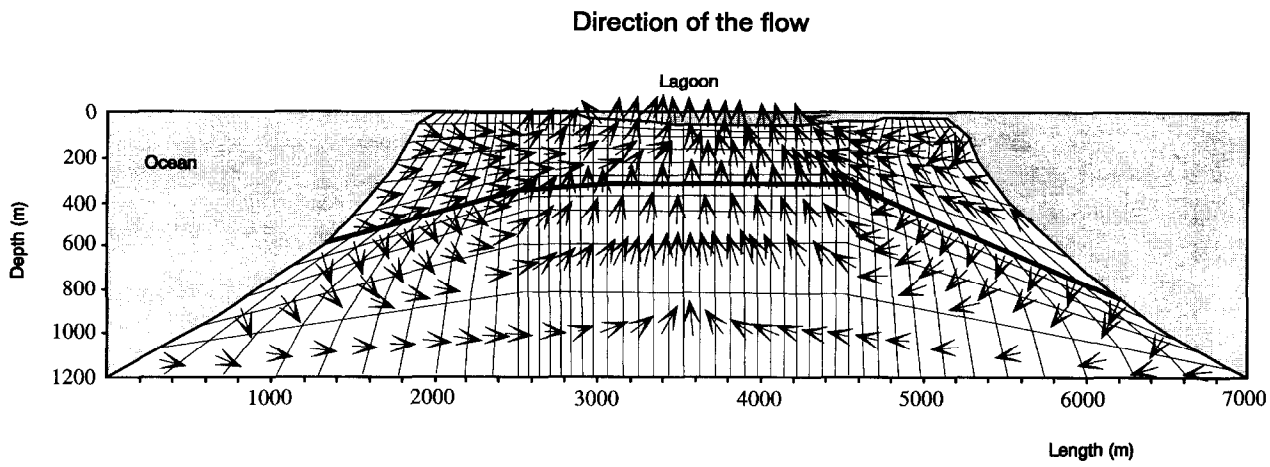

FIG. 8. Direction of steady-state fluid flow. Arrow length is constant.

of 300 m to 3 km, the time of residency of the fluids ranges from 1,000 to 10,000 years in the 10^{-13} m^2 high permeability case, and from 10,000 to 100,000 years in the more realistic 10^{-14} m^2 case. Interstitial water has been renewed many times since the end of volcanic activity 10 My ago. Original water could only be preserved where the permeability is lower than 10^{-16} m^2 (or 0.1 mD), that is only possible in the absence of a percolating fracture network.

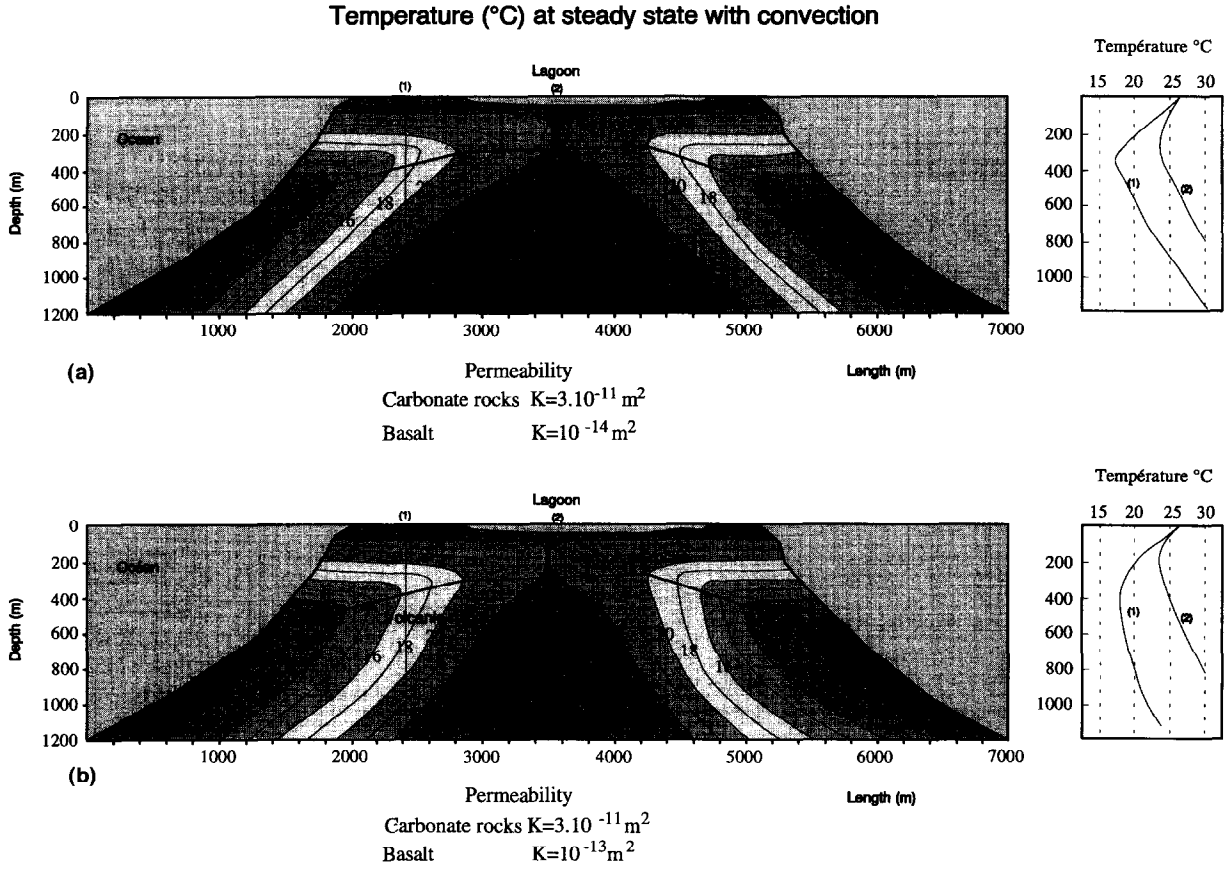

FIG. 9. Temperature field for steady-state convection and temperature profiles corresponding to (1) the reef crown and (2) the inner part of the lagoon. The temperature inversion in the carbonate section is a consequence of lateral fluid input from the ocean. Permeability in the carbonate section is 3 10^{-11} m^2. (a) with permeability 10^{-14} m^2 in the volcanic basement. (b) with permeability 10^{-13} m^2 in the volcanic basement; the cooling of the basement is due to convection. The calculations with permeability 10^{-14} m^2 fit better with the data.

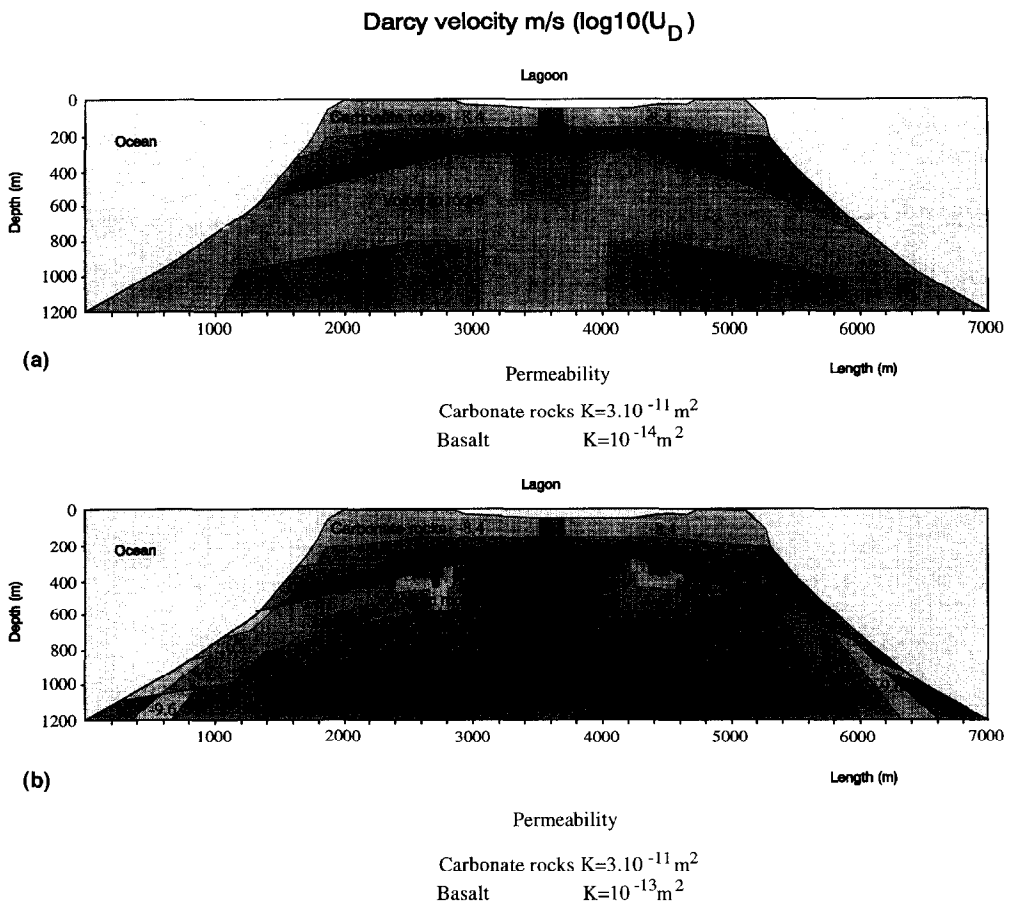

FIG. 10. Darcy velocity. The values are the decimal logarithm of the Darcy velocity, in m/s. (a) with permeability 10^{-14} m^2 in the volcanic basement. (b) with permeability 10^{-13} m^2. The response to the permeability change is almost linear.

7. MODELING OF STRONTIUM TRANSPORT

7.1. Equations and Boundary Conditions

Once the thermal convection steady state is obtained, the computed fluid velocity field is used to determine Sr concentrations from the steady-state transport Eqn. 6:

$$\nabla((\varphi d + \bar{\alpha}|U_D|)\nabla C) - U_D \cdot \nabla C + Q = 0, \quad (8)$$

where φ is the porosity, d the molecular diffusivity, and $\bar{\alpha}$ the dispersivity tensor (Table 6).

The source term Q is the mass of strontium dissolved by unit time and by unit rock volume:

$$Q = \varphi \nu S'_w [\mathrm{Sr}]_{\mathrm{glass}} \quad (9)$$

as Eqn. 6 is linear, computed concentrations are proportional to Q.

The effect of Sr adsorption on the velocity of migration is neglected. As only the steady state is considered, the amount of adsorbed Sr should stay constant and there is no need to take it into account in the equation. The boundary conditions are no Sr flux through the lower boundary and a concentration equal to that in seawater (8 ppm) on the other boundaries.

7.2. Diffusive Transport

Diffusivity of Sr in water at infinite dilution is 3.72 10^{-10} m^2/s at 0°C, 7.94 10^{-10} m^2/s at 25°C, and can be extrapolated to 10^{-9} m^2/s at 40°C (Li and Gregory, 1974). Diffusivity of Sr as a tracer in seawater (d_0) should not differ significantly from the values above (Li and Gregory, 1974) but should be lower in the altered basalt because of the tortuosity of the porous network and of the adsorption on clay surfaces. In marine sediments (including clay rich lithologies), diffusion coefficients are related to the electrical conductivity by:

$$d = d_0/F\varphi, \quad (10)$$

where d is the diffusivity in the sediment, φ is the porosity, and F is the formation factor ($F = \sigma_f/\sigma_w$), σ_f is the conductivity of the sediment and σ_w is the conductivity of the fluid (Iversen and Jørgensen, 1993; Berner, 1980). In altered basalt, however, surface conductivity is significant (Pezard, 1990) and this law does not apply rigorously, but gives an

TABLE 6. Parameters for the model of Sr transport. [a] from Guy (1989) and Guy and Schott (1989); [c] Li and Gregory (1974).

Symbol	Definition	Formula	Numerical values
v	glass dissolution rate per unit area		$2.5\ 10^{-3}$ g.m^{-2}.a^{-1} at 25°C[a]
S_w'	reactive surface area per fluid volume (i.e. glass surface)		assumed 1.6 m^2/l
C or [Sr]	strontium concentration		500 ppm in basaltic glass 8 ppm in sea-water
Q	rate of strontium liberation per rock volume	$\varphi v S_w'[\mathrm{Sr}]_{glass}$	$2\ 10^{-4}$ g.m^{-3}.a^{-1}
d_0	molecular diffusivity of strontium in water		$3.72\ 10^{-10}$ m^{2}s^{-1} at 0°C to 10^{-9} m^{2}s^{-1} at 40°C
d	molecular diffusivity of strontium in rock		10^{-9} m^{2}s^{-1} in finite element model
$\bar{\bar{\alpha}}$	dispersivity tensor	$\begin{pmatrix} \alpha_L & \alpha_T \\ \alpha_T & \alpha_L \end{pmatrix}$	$\alpha_L = 50$ m $\alpha_T = 5$ m
Pe	Péclet number (chemical)	$\frac{L.U_D}{\varphi d}$	L, fluid path length, is typically 1 km

upper bound to molecular diffusion. For mid-oceanic ridge basalt, $F \approx 10\ \varphi$ (Pezard, 1990), thus $d < d_0/10$. Assuming the same laws for Mururoa basalts, the maximum diffusivity is $d = 10^{-10}$ m^2/s in the 15–40°C temperature range. The diffuse upward flow of strontium J_{Sr} in the basalt can be estimated from Fick's Law:

$$J_{Sr} = -\varphi d \frac{dC}{dz} \qquad (11)$$

and from the concentration profiles in the drill holes (Fig. 4). Concentration gradients are of the order of 0.3 mg·l^{-1}·m^{-1}. With a porosity of 10%, $J_{Sr} = 10^{-4}$ g·m^{-2}·a^{-1}. For a minimum thickness of 100 m for the productive layer, this flow is compatible with a maximum Sr source term of $Q = 10^{-6}$ g·m^{-3}·a^{-1}, averaged over the interval, and to a rate of basalt alteration of $7.7 \infty 10^{-10}$ a^{-1}. Such a low rate is unrealistic, as it would then require more than 1 billion year to fully alter the basalt at the ambient temperature. This rapid calculation shows that the profiles cannot be the result of pure diffusion and confirms that flow of interstitial water is occurring.

7.3. Convective Transport

The chemical Peclet number computed for a 10^{-10} m^2/s diffusion coefficient, for a porosity of 10%, and for a 1 km typical path length, is about 1000 in the 10^{-14} m^2 case ($U_D = 10^{-10}$ m/s) and about 10000 in the 10^{-13} m^2 case ($U_D = 10^{-9}$ m/s). This shows that even at the low fluid velocities computed in the basement, convective transport of Sr is dominant over diffusive transport. Molecular diffusion along the flow path can be neglected for permeabilities of more than 10^{-16} m^2, corresponding to $U_D = 10^{-12}$ m/s and Pe = 10. Homogenization between aquifers by molecular diffusion is possible over a lateral distance b such that $\mathrm{Pe}(b/a)^2 < 1$ (Andrews et al., 1981; Leroy et al., 1992). Keeping the same parameters, b is 10–30 m in the modelled cases. Because these values are comparable to the depth intervals isolated for sampling, the fluid pumped out of the formation does not only represent the composition of the fluid in the fractures but should be fairly representative of the average composition of the interstitial fluid. But molecular diffusion cannot homogenize concentrations between the aquifers, which are about 100 m thick in Nerite hole (Fig. 3). In this convection dominated system, the concentration of Sr in the interstitial fluid is linearly related to the time of residency, which was estimated in this simple way.

As convective transport is largely dominant over diffusive transport, the value of the diffusion coefficient has no influence on the results. However, kinematic dispersion may be significant. As diffusion, it can be described as a random walk of tracer particles following the flow. The dispersion tensor depends on the length of the random walk step in the directions along and perpendicular to the average flow direction. In a finite element model, it should correspond to the maximum size of the heterogeneities that one cannot or do not want to describe explicitly. Consequently, it is usually absurd to make it larger than the element size. For convection dominated models the longitudinal dispersion term is mathematically equivalent to streamline diffusion and very similar to upwinding. A longitudinal dispersion coefficient of half the maximum length of the elements insures unconditional stability. In the absence of other constrains, the dispersion coefficients have here been given their minimal value compatible with numerical stability, that is $\alpha_L = 50$ m and $\alpha_T = 5$ m.

7.4. Finite Element Modeling Results

Strontium concentrations are computed in the two cases of different permeabilities from the thermal convection study, all other parameters being constant (Fig. 11). Porosity is, as previously, 10%. As the constraints on the specific surface area are poor, we adjusted the reaction rate assumed in the model to obtain computed concentrations of the same order of magnitude as the measured values (10–80 mg/L). Rate of Sr liberation per rock volume was taken equal to 2.10^{-4} g·m^{-3}·a^{-1}, corresponding to a rate of Sr concentration increase in the solution of 2.10^{-6} g·L^{-1}·a^{-1} and to a rather low $S_w' = 1.6$ m^2/L. The corresponding rate of rock alteration is $1.5\ 10^{-7}$ a^{-1} for a bulk density of 2.7 g/cm^3.

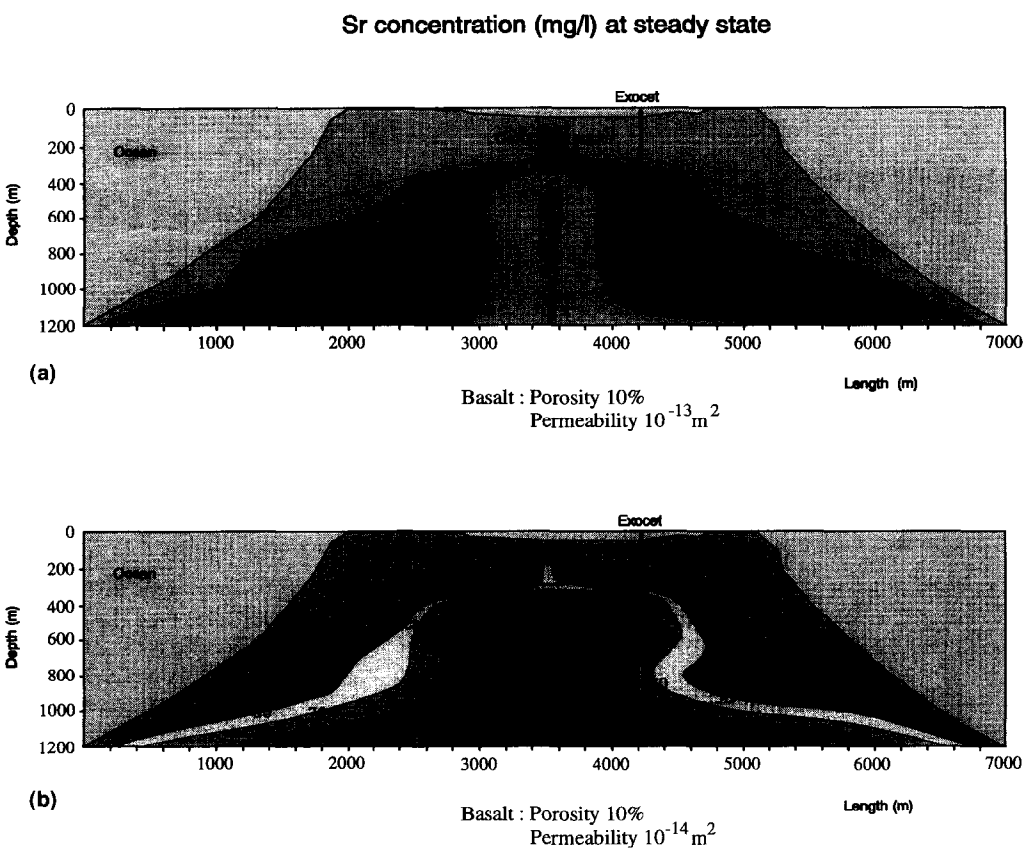

FIG. 11. Computed Sr concentration increase in porewater due to basalt dissolution. The values are in g/L. The location of Exocet drill hole on the cross-section is shown. (a) with permeability 10^{-13} m^2 in the volcanic basement. (b) with permeability 10^{-14} m^2. Note again that the response to the permeability change is almost linear. The calculations with permeability 10^{-14} m^2 fit better with the data.

This value may appear too high, as it implies total alteration in 7.5 Ma (less than the 10 Ma age of the lava flows), but this rate only applies to areas where fluid flow is presently occurring.

With the parameters above, the model using value of $k = 10^{-14}$ m^2 gives Sr concentration values in the acceptable range (20–120 ppm), but somewhat higher than measurements in Exocet drill hole (25–35 ppm). The model using value of $k = 10^{-13}$ m^2 gives concentrations about 10 times lower, in agreement with the quasi-linearity of the variation of fluid flow as a function of permeability for subcritical convection. The two models thus bracket the data. Concentrations tend to increase toward the center. This is consistent with the observation that R/W and Sr concentrations reach higher values in Nerite, situated in the center of the lagoon on the top of the volcano than in Exocet. But more probably, the difference in concentration between the drill holes is related to the difference in measured permeabilities.

7.5. Variation of Strontium Concentration with Permeability and Reaction Rate

The linear properties of the equations enable to extend the results of the two modelled cases to a wider range of parameters without additional finite element computations. Neglecting molecular diffusion, Sr concentration can be expressed as an integral of the reaction velocity along a fluid flow line. For uniform rock properties (Q, k):

$$[\mathrm{Sr}] = \frac{Q}{k}\int_0^L \mu(T)\left(\frac{dP}{ds} - \rho g \cdot t\right)^{-1} ds. \qquad (12)$$

Because of the effect of diffusive and dispersive mixing, Sr concentration in the pore fluid should depend on the average properties of the rock in a 10–100 m wide zone extending around a flow line from the ocean to the sampling point. This averaging effect should reduce the influence of local heterogeneities on the Sr concentration and justifies the use of uniform properties for a first approach. In the thermal convection model, the geometry of the model, the boundary conditions, and the thermal parameters are reasonably well constrained. Permeability k and strontium production rate Q are the main unknowns and we only consider in the following the variations of the parameters involved in their calculation (ν, $[\mathrm{Sr}]_{\mathrm{basalt}}$, S'_{w}, φ, k). Keeping constant the other parameters, the geometry of the model and the applied boundary conditions, the integral in Eqn. 8 depends only on the temperature field. When $\mathrm{Pe}_{\mathrm{thermal}} \ll 1$, thermal conduction is dominant over convective transport and the temperature field is independent of the permeability. Consequently, the fluid ve-

TABLE 7. Parameters for the model of porous medium.

Symbol	Definition	Formula	Numerical values
S_w	total physical surface area per fluid volume	$S_w = 3$ to $10\ S_w'$	> 3 m^2/l (corresponding to mm size vacuoles)
m	hydraulic radius	$1/S_w$	
a	model constant		tubes 1/5[a] to 1/8[b] cracks 2/15[b]
k	permeability	see formula (14) and (15) in text	10^{-16} to 10^{-13} m^2
φ	total porosity		1 to 10%
φ_f	fracture porosity		about 1%
S_0	vacuoles specific surface	3/<radius>	3 m^2/l
f	percolation factor		1 to 1000, depending on other parameters

[a] De Marsily (1981); [b] Gueguen and Dienes (1989).

locity field varies linearly with permeability and the integral is constant. Furthermore, we showed from the models that for $Pe_{thermal} = 1$ (corresponding to a permeability of 10^{-13} m^2) the departure from linearity is small. Therefore, the following relationship is applicable to the modeling results obtained with a permeability in the 10^{-16}–10^{-13} m^2 range:

$$[Sr] \propto \nu[Sr]_{basalt} \frac{S'_w \varphi}{k}. \quad (13)$$

The range of values for the $S'_w\varphi/k$ term that are compatible with the measured strontium concentrations is bounded by the two modelled cases ($S'_w = 1.6$ m^2/l, $\varphi = 10\%$, $k = 10^{-14}$–10^{-13} m^2). In the following section, we compare the relationship obtained between permeability, porosity, and specific surface from Eqn. 13 with a relationship based on microscopic scale models of porous media such as Kozeny-Carman's model.

8. DISCUSSION

8.1. Specific Surface and Permeability at Atoll Scale

Models of porous media either geometrical (Carman, 1937; Walsh and Brace, 1984) or based on percolation theory (Katz and Thompson, 1987; Gueguen and Dienes, 1989), generally give relationships between specific surface, permeability, and porosity of the form

$$S_w = \sqrt{af\varphi/k}, \quad (14)$$

where a depends on the model and particularly on the geometry of the individual pores, and f is a factor which is related to the probability of connection in a percolation model and to the tortuosity in a geometrical model. For an ideally connected network, $f = 1$ and f tends to zero at the percolation threshold. The tortuosity τ is defined in geometrical models by the ratio of the distance measured along the fluid path to the distance on a straight line; f is then proportional to $1/\tau^2$. The specific surface is here defined as a surface per volume of fluid and is related to the hydraulic radius m of the pores by $S_w = 1/m$ (Table 7). The assumption underlying Eqn. 14 is that m is the characteristic size of the pores that channel fluid flow. This is not true for a broad distribution of pore sizes. For example, Katz and Thompson (1987) show that in such a case the characteristic pore size relevant for permeability is about twice that relevant for electrical conductivity, and there is no general relationship linking these characteristic sizes with m.

Among the values used for parameter a, De Marsily (1981) gives $1/5$. Gueguen and Dienes (1989) show that it should be $1/8$ for a random distribution of cylindrical conduits, and $2/15$ for a random distribution of cracks. We will assume that this uncertain parameter may vary from $1/5$ to $1/8$.

More troublesome is the relationship between the total specific surface S_w and the chemically reactive surface S'_w. As discussed earlier, we have assumed that the chemically active fraction of the surface is roughly proportional to the amount of glass in the basalt, and allow S'_w/S_w to vary from $1/10$ to $1/3$. In Fig. 12a–c, the range of chemically active surface compatible with the Sr transport model is compared with the hydraulic radius from Eqn. 10 with percolation factor equal to 1. The numbers on the vertical axis correspond to $S'_w = S_w$ and the shaded zone represent the range of variation from $1/10$ to $1/3$.

For a porosity of 10% (Fig. 12a), the range of permeability in which the surface estimates are compatible is well above the maximum acceptable permeability (10^{-13} m^2). As the average permeability is more probably around 10^{-14} m^2 this implies either that the connectivity of the pore network is very low (with $f < 1/100$) or that the chemical reaction rate has been overestimated by at least one order of magnitude.

Figure 12b shows that a model with a well-connected total porosity of 1% could work with permeabilities in the acceptable range. Such a low porosity could correspond to a dense network of thin fractures (1–10 μm wide fractures spaced 100 μm–1 mm), but it is not appropriate for the bulk of the formations, as the porosity measured on samples is always more (Table 1).

A possible solution, already considered in the section on the estimation of in situ reaction rates, is that most of the porosity may correspond to surfaces that are not reactive. First, the filling of the 6% microscopic pores in the studied aerial lava flow may have formed very early by interaction with magmatic fluid during the cooling of the lavas and the surface of these pores are not necessarily active at present. Microprobe analysis show that they are generally surrounded by a thin layer having the composition of potassic feldspars, which may resist alteration. Second, vesicles generally have a radius of more than 1 mm, which gives them a very large

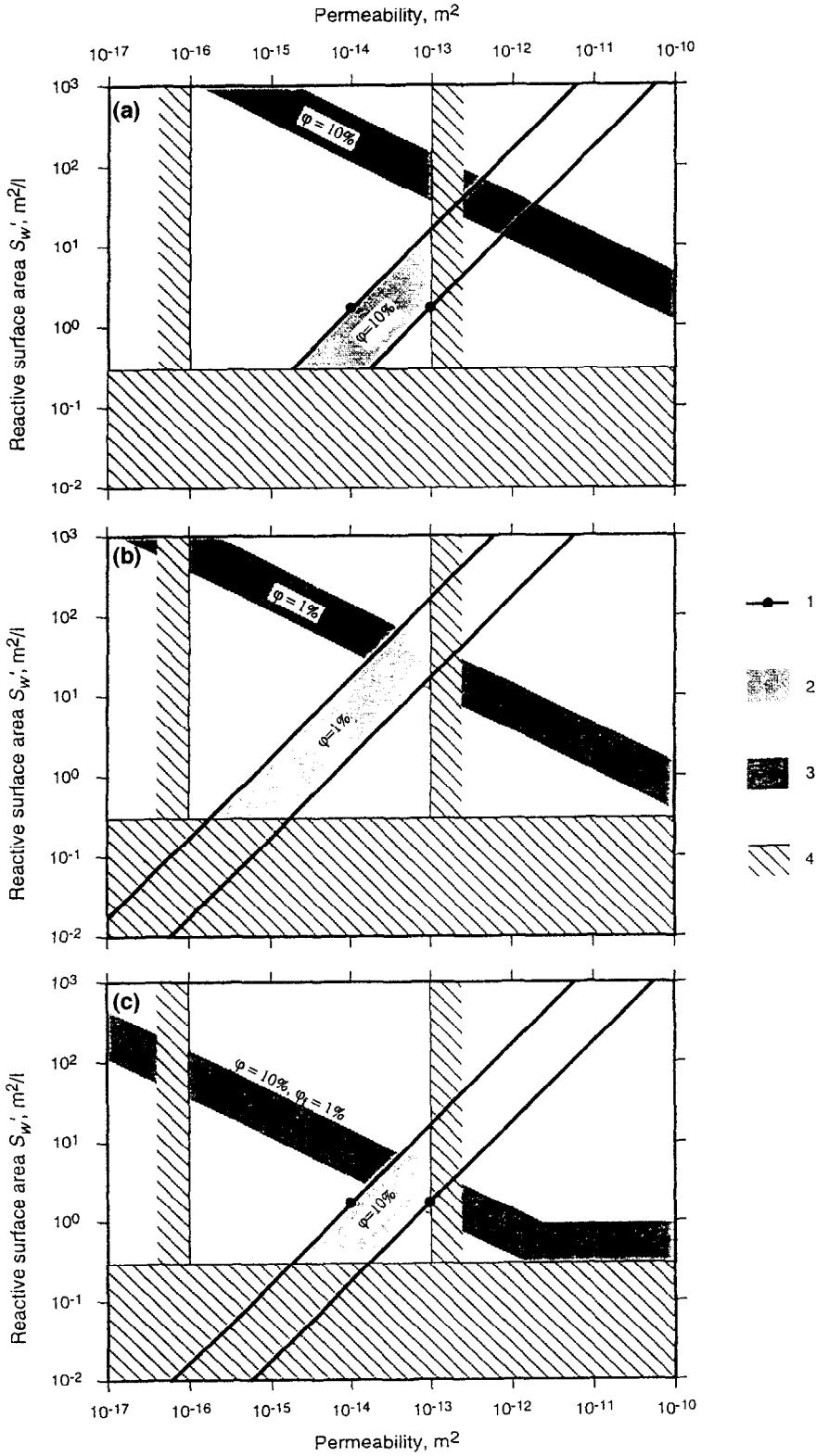

FIG. 12. Relationships between permeability and reactive surface area S'_w deduced from models. 1: Parameters of the two finite element models shown on Figs. 8–11 and their extrapolation with Eqn. 13. 2: Zone of acceptable models of Sr transport. 3: Kozeny-Carman permeability-hydraulic radius relationship (Eqns. 14, 15), for a tortuosity or a percolation factor of 1 and assuming that only $^1/_3$ to $^1/_{10}$ of the total physical surface is chemically reactive glass surface. 4: limits of acceptable values, between maximal and minimal measured permeabilities, and above a reactive

hydraulic radius compared to the connected pore network. The same reasoning applies to altered zones when they have grown larger than a few mm: they retain water which is no longer in contact with the glass. For these reasons, a model can be proposed in which about a tenth of the porosity (corresponding to 1%) is both percolating and chemically active, while the rest of the fluid acts as a buffer.

Specific surface is thus the sum of a major component corresponding to the fracture network of porosity $\varphi_f = 1\%$ and a minor one corresponding to vesicles or already replaced glass.

$$S_w = \frac{\varphi_f}{\varphi}\sqrt{\frac{af\varphi_f}{k}} + S_0. \quad (15)$$

For a vesicle radius of 1 mm, one has $S_0 = 3$ mm^{-1} = 3 m^2/L, which is about the lowest value that the specific surface can reasonably take regardless of other parameters. The resulting model (Fig. 12c) has the same permeability domain as the one with 1% total porosity and corresponds to active specific surfaces of 1–10 m^2/L. The corresponding hydraulic radius is between 10 and 100 μm. Considering 0.3 m^2/L as the minimum possible value for S'_w, the bulk permeability of the volcanics should be more than 10^{-15} m^2 in the 10% porosity case.

For any of the three configurations above, the minimum permeability compatible with this minimal estimate of reactive surface area is 10^{-16} m^2. This 10^{-16} m^2 value is the maximum permeability of sedimentary clays (Neuzil, 1994). Consequently, the clogging of fluid flow channels is probably not complete, unless the assemblages precipitated in the fractures have a much higher permeability than sedimentary clays.

Reaction rates inferred from the fluid flow model imply a lower specific surface than measurements using several independent methods. As this result is quite common in alteration studies, White and Peterson (1990) argue that the chemically reactive surface area (deduced from kinetic models based on laboratory measurements of surficial reaction rates) may be only a fraction of the physical surface area, even if only the surfaces where a chemical reaction is expected are taken into account. (1) Experimental studies of reaction rates show that the relationship between the reaction rate and the physical surface area per water volume is often nonlinear and is quite variable depending on the reaction studied and on the experimental conditions. However, it is difficult to distinguish between the effect of having a different concentration of elements in solution, and the effect of having a different reactivity of the surface. (2) Among the ten studies of reaction rates reviewed by White and Peterson (1990), eight find a physical surface greater than the reactive surface area by one order of magnitude or more. Surprisingly, this gap seems independent of the method used to estimate the physical surface area. The study of basalt dissolution in Iceland (Gislason and Eugster, 1987) is one of the two studies which fit best. Two very important characteristics of this case are the short water residence time, estimated to be a few years at most, and the young age of the system, which is not yet clogged by clay precipitation. The gap between the estimates of physical surface area and reactive surface area may increase for a more evolved or less open system. For example, Pačes (1983) proposes that naturally altered surfaces have a slower reaction rate than fresh surfaces because asperities and defects have been removed in the process of alteration, but he also mentions the role of clays in slowing the dissolution process.

In this study, we proposed solutions which do not require a change of the physical properties of the surfaces with time but require changes in the geometry of the porous network. Several factors may be involved. (1) The precipitation of clays in the fluid flow channels (spaces between clasts in brecchia, or fractures in lava flows) decreases the permeability of the network without changing the specific surface, making Kozeny-Carman's law inapplicable. (2) Alteration increases the porosity of the rock, but as most of this additional water is surrounded by secondary phases, the effect should be a decrease of the surface area per fluid volume. (3) Diffusion of silica in the fluid phase limits the rate of alteration if the altered layer is thicker than about 1 mm (Crovisier et al., 1987). In the case when fluid flow occurs only in a few unclogged fluid channels, the average distance that must be travelled by diffusion between reactive surfaces and either a drain or an empty space where precipitation can occur may be much larger than 1 mm.

In view of the available data, the choice of an explanation to the apparent discrepancy between physical surface area and chemically reactive surface area is somewhat arbitrary. The problem of the nonlinear variation of the reaction rate as a function of the surface area per volume of fluid is critical and was not addressed here. Laboratory experiments may answer this question but the whole approach also rely on the assumption, which cannot be easily checked, that laboratory measurements of dissolution rates can be extrapolated to natural cases covering a much longer period of time.

8. CONCLUSION

The presence of a temperature inversion in the carbonate section of the atoll implies lateral flow from the ocean and a high effective permeability of these carbonates that probably result from the presence of a karst system. Thermal convection within the basaltic basement of the atoll can replace the

surface area of 0.3 m^2/L (see text). The three graphs correspond to three different models of porous medium. (a) For a connected porosity of 10%. As the gap between the model and Kozeny-Carman relationship is large, the percolation factor must be small ($^1/_{10}$–$^1/_{1000}$). Unclogged paths for fluid flow are few. (b) For a connected porosity of 1% the compatibility between the models is good. However, this porosity value is too low for the bulk of the volcanic formations. (c) This case is a possible representation of a low percolation factor medium with a total connected porosity of 10%. A fracture network of porosity 1% concentrates both all fluid flow and all active surfaces. The remaining 9% of the pore space is inactive, it may correspond to vacuoles and to the interstitial porosity of clay cavities of more than a few mm diameter.

interstitial water in the upper part of the volcanic basement in a time compatible with the chemical composition of the fluids, but should not have an easily measurable effect on the temperature field. Possible times of residency for the sampled fluids range more probably between 10,000 and 100,000 years. The uncertainty on the in situ chemical reaction rates makes it difficult to give a more precise estimate.

So far as the convection model is valid, temperature data indicate that the permeability of most aquifers in the volcanic basement should not exceed a few 10 mDarcy. The minimum permeability of the bulk of the formation is more difficult to assess, but uniform permeabilities of less than 10^{-16} m^2 are not compatible with estimated alteration rates.

Extrapolation of the surficial reaction rate measured in the laboratory gives results compatible with the thermal convection model for a reactive surface area of 1–10 m^2 per liter of fluid. We measured the specific surface of samples using different methods. Combined analysis of optical and backscattering electron microscope images from the same sample is the most promising method because it allows a direct determination of the most reactive surfaces (in this case, the glass-water interface). This approach was not applied to a sufficient number of samples to give a reliable estimate of the reactive surface area. However, the image analysis shows that the rugosity of the glass alteration front is not very large. Glass alteration surfaces measured at the BEM scale (down to 0.1 μm) are at most 3.5 times larger than surfaces measured at the 100 μ scale with an optical microscope. Because the alteration front at this scale follows the fractures and veins and is concentric around vacuoles, we conclude that alteration is not causing a large increase of the physical glass-water interface.

Comparing our results with the Gislason and Eugster (1987) study of freshwater aquifers in quaternary basalts in Iceland, it is remarkable, that in spite of the 10 Ma history of alteration in Mururoa, the estimated reactive surface areas are comparable. On the other hand, permeability is at least four orders of magnitude lower in Mururoa, a decrease that can be attributed to precipitation of clay minerals in fluid flow channels. This may be representative of the evolution of basaltic formations during weathering.

Acknowledgments—We thank two anonymous reviewers for their constructive comments.

Editorial handling: G. Rich Holdren Jr.

REFERENCES

Aagaard P. and Helgeson H. C. (1982) Thermodynamic and kinetic constraints on reaction among minerals and aqueous solutions. I. Theoretical considerations. *Amer. J. Sci.* **282,** 237–285.

Andrews J. G., Richardson S. W., and White A. A. L. (1981) Flushing geothermal heat from moderately permeable sediments. *J. Geophys. Res.* **86,** 9439–9450.

Becker K., Morin R. H., and Davis E. E. (1994) Permeabilities in the Middle Valley hydrothermal system measured with packer and flowmeter experiments. *Proc. ODP, Sci. Results* **139,** 613–626.

Berger G., Schott J., and Loubet M. (1987) Fundamental process controlling the first stage of alteration of a basalt glass by seawater: an experimental study between 200°C and 320°C. *Earth Planet. Sci. Lett.* **84,** 431–445.

Berger G., Claparols C., Guy C., and Daux V. (1994) Dissolution rate of a basalt glass in silica rich solutions. Consequences for the long term. *Geochim. Cosmochim. Acta* **58,** 4875–4886.

Berner R. A. (1980) *Early Diagenesis.* Princeton Univ. Press.

Brigaud F. (1989) Conductivité thermique et champ de température dans les bassins sédimentaires à partir des données de puits. Ph.D. Thesis, Univ. Montpellier.

Brunauer S., Emmett P. H., and Teller E. J. (1938) Adsorption of gases in multimolecular layers. *J. Amer. Chem. Soc.* **60,** 309–319.

Buigues D., Gachon A., and Guille G. (1992) L'atoll de Mururoa (Polynésie française). I. Structure et évolution géologique. *Bull. Soc. Géol. Fr.* **163,** 645–657.

Carman P. C. (1937) Fluid flow through granular beds. *Trans. Inst. Chem. Eng. Lond.* **15,** 150–166.

Caroff M., Leterrier J., Maury R. C., Joron J.-L., Cotten J., and Guille G. (1992) Trace element behavior in the alkali basalt: comenditic trachite series from Mururoa atoll, French Polynesia. *Lithos* **30,** 1–22.

Crovisier J. L., Honnorez J., and Eberhart J. P. (1987) Dissolution of basaltic glass in sea water: Mechanism and rate. *Geochim. Cosmochim. Acta* **51,** 2977–2990.

Crovisier J.-L., Honnorez J., Fritz B., and J.-C. Petit (1992) Dissolution of subglacial volcanic glasses from Iceland: laboratory study and modeling. *Appl. Geochem. Suppl. Issue* **1,** 55–81.

De Marsily G. (1981) *Hydrogéologie Quantitative.* De Marsily G.

Destrigneville C. (1989) Etude de l'altération dans le massif basaltique de Mururoa (Polynésie Française): Analyses des phases solides et fluides et modélisation thermodynamique. Ph. D. dissertation, Univ. Paul Sabatier.

Destrigneville C., Schott J., Caristan Y., and Agrinier P. (1991) Evidence of an early alteration process driven by magmatic fluid in Mururoa volcano. *Earth Planet. Sci. Lett.* **104,** 119–139.

Dudoignon P., Meunier A., Beaufort D., Gachon A., and Buigues D. (1989) Hydrothermal alteration at Mururoa atoll (French Polynesia). *Chem. Geol.* **76,** 385–401.

Fang W. W., Langseth M. G., and Schultheiss P. J. (1993) Analysis and application of in situ pore pressure measurements in marine sediments. *J. Geophys. Res.* **98,** 7921–7938.

Fischer A. T. and Becker K. (1995) Correlation between seafloor heat flow and basement relief: observational and numerical examples and implications for upper crustal permeability. *J. Geophys. Res.* **100,** 12641–12657.

Gillot P.-Y., Cornette Y., and Guille G. (1992) Age (K-Ar) et conditions d'édification du soubassement volcanique de l'atoll de Mururoa (Pacifique Sud). *C. R. Acad. Sci. Paris.* **314,** Série II, 393–399.

Gislason R. S. and Eugster H. P. (1987) Meteoric water-basalt interactions. II: A field study in N.E. Iceland. *Geochim. Cosmochim. Acta* **51,** 2841–2855.

Grandstaff D. E. (1980) The dissolution rate of forsteritic olivine from Hawaiin beach sand. *Third Intl. Symp. Water-Rock Interaction,* 72–74.

Guy C. (1989) Mécanismes de dissolution des solides dans les solutions hydrothermales déduits du comportement de verres basaltiques et de calcites déformées. Ph.D. Thesis, Univ. Toulouse.

Guy C. and Schott J. (1989) Multisite surface reaction versus transport control during the hydrolysis of a complex oxide. *Geochim. Cosmochim. Acta* **78,** 181–204.

Guy C., Schott J., Destrigneville C., and Chiappini R. (1992) Low-temperature alteration of basalt by interstitial seawater, Mururoa, French Polynesia. *Geochim. Cosmochim. Acta* **56,** 4169–4189.

Gueguen Y. and Dienes J. (1989) Transport properties of rocks from statistics and percolation. *Math. Geol.* **21,** 1–13.

Hekinian R. and Hoffert M. (1975) Rate of palagonitization and manganese coating on basaltic rocks from the rift valley in the Atlantic ocean near 36°50′N. *Marine Geol.* **19,** 91–109.

Herman M. E., Buddemeier R. W., and Wheatcraft S. W. (1986) A layered aquifer model of atoll island hydrology: Validation of a computer simulation. *J. Hydrol.* **84,** 303–322.

Holdren G. R., Jr. and Berner R. A. (1979) Mechanism of feldspar weathering. I. Experimental studies. *Geochim. Cosmochim. Acta* **42,** 1161–1171.

Hyndmann R. D. and Von Herzen R. P. (1977) Heat flow measurements, DSDP leg 37. *Initial Reports DSDP* **37,** 347–362.

Iversen N. and Jørgensen B. B. (1993) Diffusion coefficients of sulfate and methane in marine sediments: Influence of porosity. *Geochim. Cosmochim. Acta* **57,** 571–578.

Join J.-L., Pomme J.-B., Coudray J., and Daessle M. (1988) Caractérisation des aquifères basaltiques en domaine littoral. Impact d'un récif coralien. *Hydrogéologie* **2,** 107–115.

Katz A. J. and Thompson A. H. (1987) Prediction of rock electrical conductivity from mercury injection measurements. *J. Geophys. Res.* **92,** 599–607.

Kozeny J. (1927) Uber kapillare Leitung des Wassers im Boden. *S.-Ber. Wiener Akad. Abt.* **136,** 271–307.

Leroy C., Hulin J.-P., and Lenormand R. (1992) Tracer dispersion in stratified porous media: influence of transverse dispersion and gravity. *J. Contaminant Hydrol.* **11,** 51–68.

Li Y.-H. and Gregory S. (1974) Diffusion of ions in seawater and deep-sea sediments. *Geochim. Cosmochim. Acta* **38,** 703–714.

Maury R. C. et al. (1992) L'atoll de Mururoa (Polynésie française). II: La série magmatique. *Bull. Soc. Géol. Fr.* **163,** 659–679.

Neuzil C. E. (1994) How permeable are clays and shales? *Water Resources Res.* **30,** 145–150.

Oberdorfer J. A., Hogan P. J., and Buddemeier R. W. (1990) Atoll island hydrogeology: Flow and freshwater occurrence in a tidally dominated system. *J. Hydrol.* **120,** 327–340.

Pačes T. (1983) Rate constants of dissolution derived from the measurements of mass balance in hydrological catchments. *Geochim. Cosmochim. Acta* **47,** 1855–1863.

Pezard P. (1990) Electrical properties of mid-ocean ridge basalt and implications for the structure of the upper oceanic crust in hole 504B. *J. Geophys. Res.* **95,** 9237–9264.

Robert C. and Goffé B. (1993) Zeolitization of basalts in subaqueous freshwater settings: Field observations and experimental study. *Geochim. Cosmochim. Acta* **57,** 3597–3612.

Rougerie F. and Wauthy B. (1993) The Endo-upwelling concept: from geothermal convection to reef construction. *Coral Reefs* **12,** 19–30.

Samaden G., Dallot P., and Roche R. (1985) Atoll d'Eniwetok. Système géothermique insulaire à l'état naturel. *La Houille Blanche* **2,** 143–151.

Scheidegger A. E. (1972) *The Physics of Flow Through Porous Media.* Univ. Toronto Press.

Schott J., Berner R. A., and Sjöberg E. L. (1981) Mechanism of pyroxene and amphibole weathering. I. Experimental studies of iron-free minerals. *Geochim. Cosmochim. Acta* **45,** 2123–2135.

Velbel M. A. (1985) Geochemical mass balances and weathering rates in forested watersheds of the southern blue ridge. *Amer. J. Sci.* **285,** 904–930.

Walsh J. B. and Brace W. F. (1984) The effect of pressure on porosity and the transport properties of rock. *J. Geophys. Res.* **89,** 9425–9431.

Weidel E. R. (1980) *Stereological Method,* Vol. 2. Academic Press.

White A. F. and Peterson M. L. (1990) Role of reactive-surface-area characterization in geochemical kinetic models. In *Chemical Modelling of Aqueous Systems II; ACS Symp. Series* **416,** 461–475.